International Journal of Coal Science & Technology (2023) 10:40
https://doi.org/10.1007/s40789-023-00600-w

RESEARCH

Coal petrology, sedimentology and depositional environment of the Parvadeh coals in the Upper Triassic, Tabas Block of Central-East Iran

Ziba Zamani[1] · Hossain Rahimpour-Bonab[1] · Ralf Littke[2]

Received: 10 October 2022 / Revised: 21 December 2022 / Accepted: 15 June 2023
© The Author(s) 2023

Abstract
Peat forming environment strongly influences the economic value of any coal seam and coal-bearing strata. Hence, palaeoenvironmental studies provide important information for coal resource exploration. In this context, detailed studies on selected coals from the Parvadeh Area, Iran, were conducted using sedimentology, coal petrology, X-ray diffraction (XRD), scanning electron microscopy- energy dispersive X-ray analyzer (SEM-EDX), and proximate analysis. The sedimentary facies above and below the coal seams are mainly marine or marine-influenced facies, supporting that the coal-forming mires in the Parvadeh Area developed in a paralic environment, where the base level must be closely related to sea level. Sulfur contents are moderate to high and mark the influence of brackish/marine water, especially during transgression after peat growth in a lower delta plain environment. The peat-forming mires extended on coastal/delta plain lobes. The lower delta plain/coastal plain coals are characterized by lateral continuity and substantial thickness, whereas few coals possibly representing the upper delta plain are thin and more discontinuous. The detrital nature and composition of the numerous partings and the overall high ash yield in the coal seams indicate an active tectonic area with high rates of creation of accommodation space over peat growth. Coal petrology and coal facies analysis exhibits a permanently high water table within a forest swamp and mostly rheotrophic conditions, sometimes with connection to the seawater. According to paleoenvironmental reconstructions, it seems that coal layers may be thicker, with less sulfur (pyrite), but more clastic minerals and partings toward the western part of the area. Although these coal seams presently have low economic potential for the mining operation, partly due to great depth, this humic, high-volatile to medium-volatile bituminous coal may be suitable for exploration of coal bed methane resources.

Keywords Coal petrology · Sedimentology · Coal facies analysis · Upper Triassic · Nayband Formation · Tabas Block

1 Introduction

For many centuries, coal has been one of the most important fossil fuels globally; more recently, it was also recognized that it is an important source rock for natural gas and – less commonly – for oil and even a reservoir for unconventional gas resources, i.e. coal-bed methane. Depositional models are considered a standard tool for coal explorations and mine production planners. These models aim to establish relationships between the coal distribution, quality parameters, and the sedimentological characteristics of the palaeoenvironment of peat swamps (Hagelskamp et al. 1988; Littke and Zieger 2019). Coal formation, preservation, and quality are strongly affected by variations in sedimentary environments (McCabe 1987; Fielding 1987). The main economic characteristics of coal are its thickness, lateral continuity, geometry, rank, maceral type, and mineral content. Other than rank, the remaining properties are influenced by the mire. Therefore, paleoenvironmental interpretation allows predicting coal quality in an area. Furthermore, plotting coal quality data indicates the distribution of different properties and helps to decipher the paleoenvironmental influences that existed during coal depositional and post-depositional processes.

Establishing the stratigraphic and sedimentological framework in an area is useful both for predicting the features

✉ Hossain Rahimpour-Bonab
rahimpor@ut.ac.ir

[1] School of Geology, College of Science, University of Tehran, Tehran, Iran

[2] Energy and Mineral Resources (EMR), RWTH Aachen University, Aachen, Germany

of the same stratigraphic section in adjacent, less explored areas and for evaluating older, less well-known deposits at greater depth. The results of these studies are used to predict best-drilling sites and reduce the number of exploration boreholes required, which are the primary investigative tools used by coal mining companies to date (Hagelskamp et al. 1988). Peat swamp formation, development, and their stratigraphic position are primarily controlled by the same mechanisms as terrestrial clastic sediment deposits; i.e. there is a strong control by climate and accumulation space (McCabe 1987; Diessel 1992; Wadsworth 2010). It is possible to establish a stratigraphic framework for a coal-bearing setting in two ways: by examining the sedimentary succession in which the coals occur and by studying the coals themselves (Thomas 2002). All these studies have certain limitations. It is, therefore, essential to embark on a multidisciplinary and multi-technical approach to develop a robust paleoenvironmental interpretation (McCabe 1987; Kalkreuth et al. 1991; Scott 2002; Sen 2016; Stock et al. 2016; Dai et al. 2020). Therefore, in this study, both the sedimentological framework and the coal petrology were investigated for the Rhaetian coal-bearing Qadir member of the Nayband Formation of Central-East Iran (Fig. 1).

2 Geological background

2.1 Location, boundaries and structural overview

The major coal seams of Iran, with about 7–10 billion tons reserves, are part of the Upper Triassic to Middle Jurassic Shemshak Group and are spread over northern, central, and eastern Iran (Zadehkabir 1994a; Shariat Nia 1994; Moinosadat and Razavi Armaghani 1994). Two coalfields are under operation in Central Iran and another one along the Alborz Mountain Range. The central basin, known as the Tabas Coal Basin, contains four coal mines, namely Parvadeh, Nayband, Mazino, and Abdoughi. It is the largest and richest coal basin in Iran. In terms of reserves, the Tabas Basin has 69% of coking coal, 99% of thermal coal, and 75% of Iran's total defined coal resources (Fallah 2018).

The Parvadeh coal mine is located in the Tabas Block, in the central part of the Central Eastern Iranian Microcontinent (CEIM). The CEIM consists of three north-south oriented structural blocks, Lut, Tabas, and Yazd blocks, from east to west, respectively (Fig. 1a). These blocks are separated by linear to curvilinear N-S right lateral strike-slip active faults. The Tabas Block is a spindle-shaped intracontinental depression bounded by the active Nayband Fault in the east and the Kalmard-Kuhebanan Fault in the west (Konon et al. 2016). The subsidence along these faults was considerable from Late Triassic to Early Cretaceous and resulted in strong sedimentation on the Tabas Block (Saidi et al. 1997). The block exhibits very thick and well exposed Upper Triassic-Jurassic successions (Fig. 1b). The primary coal-bearing Qadir member in the Parvadeh coal mine has a good outcrop in this area (Fig. 2a) and contains seven coal seams, namely A, B1, B2, C1, C2, D, and E from base to top. Commonly their depth, thickness, ash yield and rank increase from east to west (Shariat Nia 1994).

The Parvadeh coal mine with an area of 1200 km^2, is located about 75 km south of Tabas City. It is bounded by

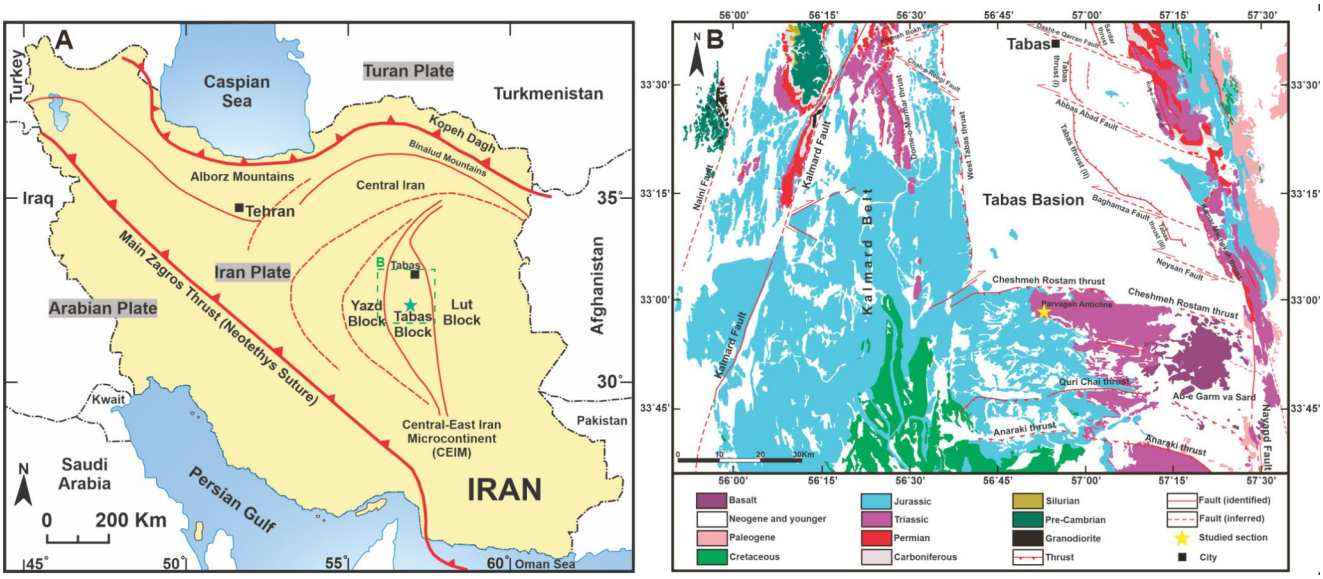

Fig. 1 **a** Simplified structural and geographical framework of Iran showing the main sutures, structural units and geographical area (redraw from Wilmsen et al. 2009b) **b** Geological map from a part of northern Tabas Block (redraw from Konon et al. 2016). The studied area is indicated by an asterisk in the Figures

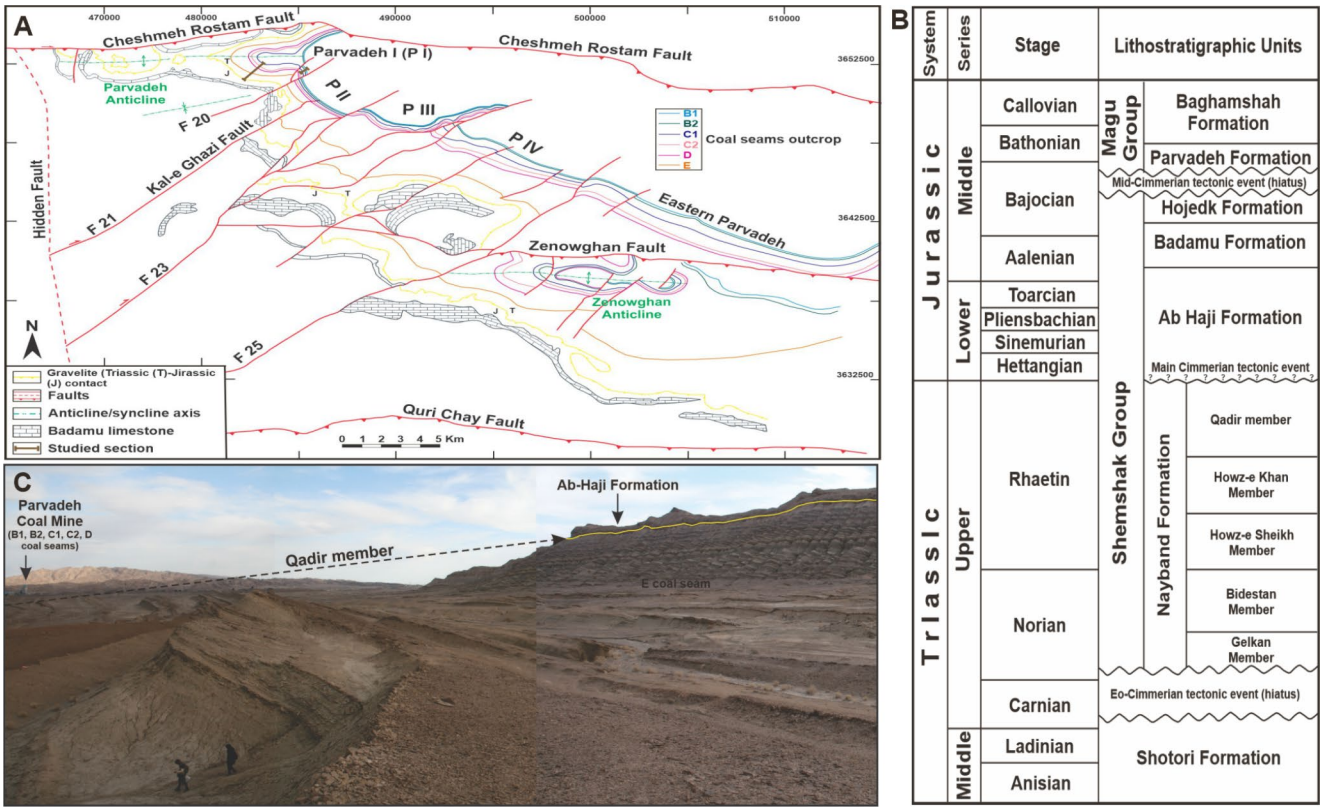

Fig. 2 **a** Structural blocks and coal seams outcrop in the Parvadeh Area (modified after Shariat Nia 1994 and Shariat Nia et al. 1997). The location of the studied section is indicated on the map **b** Main lithostratigraphic units of the Middle Triassic to Middle Jurassic successions in the Parvadeh Area. (Modified from Seyed-Emami 2003 and Wilmsen et al., 2009) **c** Distance panorama field view of the Qadir coal-bearing measured section in the Parvadeh coalmine area, view is to the southeast

the northern and southern Cheshmeh Rostam and Quri Chay faults, respectively, the Nayband fault to the east and a concealed fault to the west (Fig. 2a). The Nayband fault and its splay NE-SW strike-slip faults - such as Cheshmeh Rostam and Quri Chay - govern the tectonism of the area (Shariat Nia 1994; Konon et al. 2016; Nazemi, 2018) (Figs. 1b and 2a) and segment the area into distinct blocks. As a result, the area has been divided into smaller areas, which from west to east are referred to as Parvadeh I (PI), II (PII), III (PIII), IV (PIV), and Eastern (PE) (Fig. 2a). A series of monocline anticlines with east-west trending fold axes are developed in proximity to these faults. This low-dipping (5° to 15°) monocline style is preserved over large parts of the region and provides persistent, low-dipping, and relatively undisturbed mining blocks (Shariat Nia 1994; Nazemi, 2018). One characteristic of the Parvadeh coals is high methane gas content, i.e. more than 10 m^2/tone coal from 100 m and deeper (Molayemat and Mohammad Torab 2017).

2.2 Tectonics and paleogeography

The structural history and sedimentary development of the Triassic in Iran are primarily governed by Cimmerian Orogenesis (Seyed-Emami, 2003). The closure of the Paleo-Tethys and the opening of Neo-Tethys at the expense of the Paleo-Tethys caused accretion of the Iranian plate to the southern margin of Eurasia (Turan Plate) that, in turn, led to the Early Cimmerian Orogeny (Fig. 3) (Davoudzadeh and Schmidt 1984; Saidi et al. 1997; Cifelli et al. 2013). The closure of the Paleo-Tethys and the continent-continent collision caused significant uplift along the Iranian plate, in the northern margin, turning it into an underfilled Carnian-Rhaetian flexural foreland basin (Wilmsen et al. 2009a, b) (Fig. 3). At the same time, the subduction of Neo-Tethys started at the southern edge of the plate (Wilmsen et al. 2009a, b), which reduced the compression of the Iranian plate and initiated the subsequent formation of extensional basins and sea transgression onto the CEIM. These basins were filled at the expense of high-relief erosion and caused

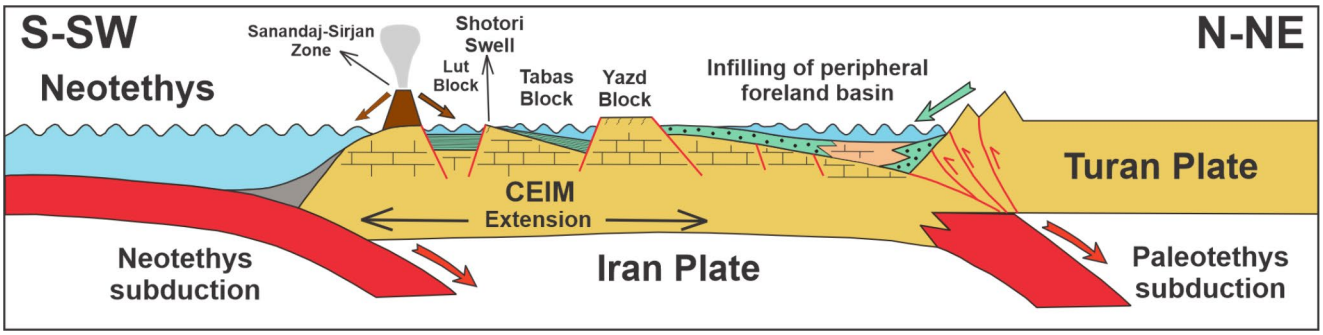

Fig. 3 Geodynamic sketch of the Late Triassic (Middle Norian-Rhaetian) effects of the Cimmerian Orogeny on the Iran Plate. (modified from Wilmsen et al. 2009b; Cifelli et al. 2013)

deposition of about 3000 m Nayband and other formations of the Shemshak Group (Davoudzadeh and Schmidt 1984; Seyed-Emami 2003; Fürsich et al. 2005). The rupture of the slab at the Triassic-Jurassic boundary caused a rapid uplift of the Cimmerides and sea level regression. It resulted in the non-deposition or erosion in the most parts of the CEIM, e.g. in the Parvadeh area, before deposition of the Lower Jurassic Ab Haji Formation started (Fig. 2b).

2.3 Stratigraphy

The Nayband Formation is the oldest stratigraphic unit of the Shemshak Group in Central Iran (Fig. 2b) and is well-developed on the Tabas Block. At the same time, it is present only in some regions of the Lut Block and missing in the Yazd Block (Fürsich et al. 2005). These sediments overlie the Middle Triassic carbonates of the Shotori Formation with an erosional unconformity and ancient karst (Seyed-Emami 2003). In the Nayband type section, on the southern flank of the Nayband Mountain, this formation is 2195 m thick (Brönnimann et al. 1971), and its overall thickness diminishes from the type section to the north (Fürsich et al. 2005). This formation is subdivided from bottom to top into four siliciclastic-carbonate members; Gelkan Member, Bidestan Member, Howz-e Sheikh Member, and Howz-e Khan Member (Fig. 2b). In the Parvadeh area, the lithology of the Nayband Formation is changing, and the thicknesses are much lower (Repin 1985). In addition, the top carbonate member (Howz-e Khan Member) is partially or entirely replaced by a thick siliciclastic coal-bearing succession. This unit was informally nominated by the National Iranian Steel Cooperation geologists as Qadir member (Shariat Nia 1994).

A complete section of the siliciclastic Qadir member with prominent coal is present in the Parvadeh area. Its thickness reaches more than 1000 m, with lithologies similar to the type section (Shariat Nia 1994). At the top of the Qadir member, there is a clear border with the overlaying Ab-Haji Formation (Fig. 2c). At the base of the Ab-Haji Formation there are some coarse-grained sandstones of variable thickness forming a micro-conglomerate called the "Gravellite" horizon. The bottom of this bed is defined as the Triassic-Jurassic border (Shariat Nia 1994; Seyed-Emami 2003; Wilmsen et al. 2009a; Salehi et al. 2015). Based on a study of floral fossils (Vassilev 1984) it was concluded that there is a stratigraphic gap between the Qadir member and the Ab-Haji Formation (Fig. 2b). According to paleontological studies in this area, the age of the Qadir member is Rhaetian (Vassilev 1984; Jalalifard et al. 2011; Vaez-Javadi 2012; Ghavidel-Syooki et al. 2015; Sabbaghiyan et al. 2020). Paleontological as well as sedimentological studies show deltaic to shallow marine sedimentary environments, as well as a tropical to subtropical climate with a progressive decrease in temperature during the Upper Triassic (Moinosadat and Razavi Armaghani 1994; Shariat Nia 1994; Fürsich et al. 2005; Vaez-Javadi 2012; Ghavidel-Syooki et al. 2015; Sajjadi et al. 2015; Zamansani et al. 2019; Zamaniyan et al. 2018). In addition, organic petrographic and geochemical investigations of this coal-bearing sequence in the Tabas Block show the presence of kerogen type III and humic coals in the oil to the gas window and corresponding low volatile bituminous to anthracite coalification stages (Moinosadat and Razavi Armaghani 1994; Shariat Nia 1994; Zadehkabir 1994b; Alizadeh et al. 2011; Hashemi 2012; Ghavidel-Syooki et al. 2015; Zamansani et al. 2019).

3 Methodology

3.1 Field studies and sampling

Along a stratigraphic section, the Qadir member was studied and described in the southeast and west of the Parvadeh Anticline (56°48'56", 33°0'27"), where this member is accessible and exposed (Fig. 2a, c). The base of this section (bottom of B1 coal seam) is covered by mining activity and the top of it is disconformably overlain by the Ab-Haji Formation (Fig. 2b, c). During the field studies, various

parameters were determined such as size, texture, composition, lithology, thickness, fossils, bedding nature, bed geometry, continuity, sedimentary structures, and lateral and vertical facies changes.

Coal sampling was carried out both in underground coal mines and outcrops (along stratigraphic sections). Twenty-one coal samples were collected from underground mines of B1, B2, C1, and C2 coal seams with the pillar coal sampling method and blocks of coals from working faces of mine; samples were initially stored in a hermetically sealed plastic bag (Table 1). The coals sampled in the outcrops were first excavated from a depth of more than 1 m to remove weathered material. Surface coal samples were from B1, B2, C1, C2, D, and E coal seams.

3.2 Organic petrography

For organic petrographic analysis, coal samples were crushed to about 1 mm size and embedded in a two-phase mixture of resin and hardener (Araldite) at the rate of 10:3. After hardening, the sample blocks were ground flat and polished in different stages with silicon carbide and fine-grained alumina powder to obtain a clean, uniformly flat, and scratch-free surface (Taylor et al. 1998; ISO 7404-2 2009). Microscopic investigations were carried out with a Leica-MPV-COMBI microscope under white incident and blue light excitation (fluorescence) using a 50x oil immersion objective; thus a 500x magnification was reached. The microscope has a photomultiplier, digital readout, and a computer attached to process the data. The petrographic analysis includes maceral counting and vitrinite reflectance

Table 1 Data of the samples from Parvadeh coalmine area

Sample name	Type	Thickness (m)	Lithology	Mine	Coal seam
QP 1	Surface Sample	0.3	Coal	Parvadeh 1 (PI)	B1
QP 5	Surface Sample	11.8	Ash coal	Parvadeh 1 (PI)	B1
QP 8	Surface Sample	37	Coal	Parvadeh 1 (PI)	B2
QP 14	Surface Sample	57.5	Coal	Parvadeh 1 (PI)	C1
QP 19	Surface Sample	110.9	Coal	Parvadeh 1 (PI)	C2
QP 20	Surface Sample	122.2	Coal	Parvadeh 1 (PI)	D
QP 53	Surface Sample	393	Coal	Parvadeh 1 (PI)	E
Q-PI-CM-C1	Subsurface-Pillar sampling		Coal	Parvadeh 1 (PI)-Central Mine	C1
Q-PI-CM-C1-Block	Subsurface-Block sample		Coal	Parvadeh 1 (PI)-Central Mine	C1
Q-PI-CM-B2	Subsurface-Pillar sampling		Coal	Parvadeh 1 (PI)-Central Mine	B2
Q-PII-N-C1	Subsurface-Pillar sampling		Coal	Parvadeh 2 (PII)	C1
Q-PII-N-C1-Block	Subsurface-Block sample		Coal	Parvadeh 2 (PII)	C1
Q-PII-N-B1	Subsurface-Pillar sampling		Coal	Parvadeh 2 (PII)	B1
Q-PII-N-B1-Block	Subsurface-Block sample		Coal	Parvadeh 2 (PII)	B1
Q-PII-N-B2	Subsurface-Pillar sampling		Coal	Parvadeh 2 (PII)	B2
Q-PII-N-B2-Block	Subsurface-Block sample		Coal	Parvadeh 2 (PII)	B2
Q-PIII-E12-C1	Subsurface-Pillar sampling		Coal	Parvadeh 3 (PIII)	C1
Q-PIII-E12-C1-Block	Subsurface-Block sample		Coal	Parvadeh 3 (PIII)	C1
Q-PIII-W8-B2	Subsurface-Pillar sampling		Coal	Parvadeh 3 (PIII)	B2
Q-PIII-W8- B2-Block	Subsurface-Block sample		Coal	Parvadeh 3 (PIII)	B2
Q-PIV-E1-C1	Subsurface-Pillar sampling		Coal	Parvadeh 4 (PIV)	C1
Q-PIV-E1-C1-Block	Subsurface-Block sample		Coal	Parvadeh 4 (PIV)	C1
Q-PE-E2 (RE)-C1	Subsurface-Pillar sampling		Coal	Eastern Parvadeh (PE)	C1
Q-PE-E2-C1-Block	Subsurface-Block sample		Coal	Eastern Parvadeh (PE)	C1
Q-PE-E2 (UD)-C1	Subsurface-Pillar sampling		Coal	Eastern Parvadeh (PE)	C1
Q-PE-E2 (LD)-C1	Subsurface-Pillar sampling		Coal	Eastern Parvadeh (PE)	C1
Q-PE-E2 (L)-C1	Subsurface-Pillar sampling		Coal	Eastern Parvadeh (PE)	C1
Q-PE-E2 (R)-C1	Subsurface-Pillar sampling		Coal	Eastern Parvadeh (PE)	C1

measurements. At least 500 points were counted per sample with equal distance between the points during the maceral analysis, and the maceral composition (Table 2) is expressed as volume percent (vol%) according to ISO 7404-3 (2009). Maceral classification used in this study referred to ICCP (1998), ICCP (2001) and Pickel et al. (2017).

Mean random vitrinite reflectance measurement (VRr) was performed in a dark room on at least 50 points per sample following ISO 7404-5 (2009). Before measurement, two mineral standards of known reflectance were used for microscope calibration, i.e., Spinel (0.423%) and Gadolinium-Gallium-Garnet (GGG, 1.716%).

3.3 Experimental bulk analysis

Nine coal samples were selected for X-ray diffraction (XRD) analysis to identify the type and amounts (semi-quantitative) of major and some minor minerals (Table 3). This measurement was performed on sample powder and carried out using a Philips PW1800 diffractometer with Cu K-alpha radiation. XRD analysis was done on raw coal samples without an ashing process to concentrate the mineral matter. Ashing causes the formation of artifact minerals due to high-temperature heating and oxidation (Ward 2002). The XRD pattern obtained from raw coal had a relatively high organic matter background (Ward 2002). Still, due to the medium to high ash yield of the Parvadeh coals (Shariat Nia 1994), the mineral pattern is discernable in the diffractograms of the coal with a relatively high proportion of crystalline minerals. Another experimental method that was applied is scanning electron microscopy (SEM) allowing the identification of minerals in a multicomponent system, such as coal, which is otherwise complex and insecure for minor minerals due to XRD detection limits (generally at about 0.5%–1.0%) and peak overlapping (Mishra et al. 2016). This technique was also performed for microstructural and microtextural observations on the coals. The fresh surface of 10 samples was coated with gold powder and investigated using a TESCAN-VEGA II XMU instrument, equipped with an energy dispersive X-ray analyzer (EDX).

In order to determination of some compounds, coals was analyzed by proximate analysis (21 samples). It consists of a particular group of tests used widely as the basis for coal utilization, determination of the general coal properties, and assessing the quality of coal (Diessel 1992; Thomas 2002; Speight 2015). The analysis is performed to measure the moisture, volatile matter, ash yield, and fixed carbon yield by a series of standard test methods. Before the examination, the samples were pulverized to a fine powder (about 0.2 mm) using a rotational mill. To determine each parameter, samples should be weighed before and after the heating stages. For moisture measurement, one gram of the sample was heated for 8 h at 105 ˚C, then the sample was weighed, and the lost weight was considered as moisture content (ISO 589 2008). The heating program for ash yield measurement is one-hour heating at 500 ˚C and one hour at 815 ˚C (ISO 1171 2010). According to the ISO 562 (2010) standard for volatile matter determination, a water-free sample (~ 1 gr) is heated for 7 min in a furnace at 900˚C. The fixed carbon content was calculated by difference based on the above results (Table 4). All of these analyses were repeated three times for each sample.

4 Sedimentological characteristics of coal-bearing sequences

All the sedimentological signatures gathered along the stratigraphic surface section show that the coal-bearing intervals belong to the delta/coastal plain environment. Besides coal seams, some of the most critical indicators are thick fine-grained lithofacies containing plant fossils and organic matter. They are interbedded with thin to medium thickness siltstone and very fine to fine-grained sandstone with tabular and planar cross-stratification, wave and current ripple marks, and sheet-like geometry (Fig. 4a–d, g). Distributary channels in these intervals are characterized by relatively thick sandstone bodies with lower sharp erosive concave boundaries and with a subtle upward-finning trend (Fig. 4d). The thickness of the delta plain setting varies from 15 to 60 m, and layers of coal and carbonaceous fine-grained siliciclastics occur at the base of small coarsening upward cycles that are often topped by thin sandstones containing marine fossils and/or trace fossils, which invoke sea level transgression on the lower coal-bearing succession. The presence of wave ripple marks, marine fossils, and trace fossils (e.g., *Arenicolites, Rhizocorallium*) (Fig. 4e, f), heterolithic and hummocky structures, and marine dinoflagellate cysts (Sabbaghiyan et al. 2020) indicates the marine influence on this part of the delta (Miall 2000).

Coal seams occur at the base and in the upper part of the studied surface section (Fig. 2c). The thickness of coal seams ranges from centimeters up to 3 m (Fig. 4d, g, h). They usually have gradual contacts at the base and sharp contacts at the top. The sharp contacts above the coal seams indicate removal of a part of the peat precursor due to switching fluvial channels or torrential crevasse floodings from the channels. Gradational contacts below coal seams indicate a continuum of deposition and genetic relationship between the siliciclastic sedimentary and coal facies. There are many plant fossils on the surface of coal layers (Fig. 4b).

Coals commonly are laminated and shiny due to vitrain and clarain lithotypes (Fig. 4i), and interlayered with several organic-rich partings consisting of fine-grained siliciclastics

Table 2 Results of coal petrology (maceral and mineral composition, random vitrinite reflectance) and coal facies indices

Sample name	Vitrinite (vol%)*					Liptinite (vol%)*				Inertinite (vol%)*					MM (vol%)	A/I	VRr (%)	GI	TPI	GWI_{AC}	VI
	V1	V2	V3	V4	V	L1	L2	L3	L	I1	I2	I3	I4	I							
QP 1	22.9	53.2	2.8	16.1	95.0	0.0	1.0	0.0	1.0	1.4	0.0	0.6	2.0	4.0	33.6		1.2	28.2	2.4		
QP 5	3.5	85.7	2.2	4.0	95.4	0.0	0.0	0.3	0.3	0.8	0.0	0.3	3.2	4.3	33.6		1.15	23.9	4.9		
QP 8	3.2	81.2	1.2	4.4	90.0	0.0	0.0	0.0	0.0	2.0	0.0	0.9	7.1	10.0	43.1		1.03	9.9	3.4		
QP 14	14.9	55.6	1.0	6.4	77.9	0.4	0.0	0.0	0.4	10.0	0.0	1.9	9.8	21.7	35.5		0.97	4.0	2.8		
QP 19	6.7	82.4	1.6	4.6	95.3	0.0	1.0	0.0	1.0	1.6	0.0	0.7	1.4	3.7	35.7		1.03	32.1	6.0		
QP 20	8.3	75.6	1.2	4.4	89.5	0.0	0.0	0.0	0.0	1.3	0.0	1.5	7.7	10.5	28.2		0.84	10.0	3.2		
QP 53	9.4	55.8	0.0	5.1	70.3	0.2	0.2	0.2	0.6	18.0	0.0	1.9	9.2	29.1	25.0		0.79	2.7	3.4		
Q-PI-CM-C1	6.5	59.5	8.5	8.3	82.8	0.0	1.0	0.5	1.5	11.3	0.0	1.6	2.8	15.7	18.3	0.7	1.35	6.0	2.2	3.2	4.2
Q-PI-CM-C1-Block	5.3	62.3	3.5	2.9	74.0	0.0	1.5	0.5	2.0	6.8	0.0	6.5	10.7	24.0	2.4	0.7		4.6	1.8	2.4	3.2
Q-PI-CM-B2	4.2	78.2	7.4	3.2	93.0	0.0	1.4	0.3	1.7	3.0	0.0	0.7	1.6	5.3	13.0	0.9	1.4	20.3	3.6	9.2	9.4
Q-PII-N-C1	5.5	61.6	8.4	10.5	86.0	0.0	2.0	0.5	2.5	5.7	0.0	2.0	3.9	11.6	37.5	0.8	1.25	9.2	1.7	4.6	3.0
Q-PII-N-C1- Block	10.1	58.1	1.3	4.3	73.8	0.0	0.5	0.0	0.5	18.3	0.1	2.9	4.4	25.7	9.4	0.7		3.4	4.4	1.7	6.6
Q-PII-N-B1	5.4	66.0	3.6	4.1	79.1	0.5	1.1	0.4	2.0	13.2	0.1	2.7	2.9	18.9	13.9	0.6	1.3	5.1	3.9	2.4	6.7
Q-PII-N-B1- Block	6.6	74.4	0.0	2.8	83.8	1.0	1.0	0.5	2.5	6.2	0.1	1.9	5.5	13.7	3.0	0.7		7.4	5.0	3.2	5.2
Q-PII-N-B2	3.4	75.1	5.0	10.6	94.0	0.0	1.0	0.5	1.5	1.4	0.0	0.3	2.8	4.5	23.0	1.0	1.26	22.5	2.3	13.5	3.1
Q-PII-N-B2- Block	0.8	78.4	1.7	7.5	88.4	0.0	1.5	0.5	2.0	2.5	0.0	1.5	5.6	9.6	20.0	0.9		11.2	2.6	14.4	3.2
Q-PIII-E12-C1	8.1	72.9	10.9	2.8	94.7	0.0	0.5	0.5	1.0	1.1	0.1	0.7	2.4	4.3	8.5	0.9	1.08	26.3	2.7	5.4	8.1
Q-PIII-E12-C1-Block	3.3	79.7	0.0	3.3	86.3	0.0	1.5	0.5	2.0	5.0	0.3	1.5	4.9	11.7	2.2	0.7		8.6	5.0	5.0	5.7
Q-PIII-W8-B2	4.1	63.7	4.6	18.3	90.7	0.0	1.0	0.5	1.5	4.1	0.0	0.5	3.2	7.8	34.5	0.8	1.2	12.5	1.5	7.6	1.9
Q-PIII-W8-B2-Block	6.9	41.0	5.3	6.0	59.2	0.0	1.0	0.5	1.5	34.6	0.5	0.9	3.3	39.3	34.1	0.6		1.6	4.0	1.3	6.5
Q-PIV-E1-C1	6.5	66.0	1.6	4.6	78.7	0.0	2.9	0.6	3.5	6.0	0.0	4.3	7.5	17.8	3.2	0.7	1.18	6.2	2.5	2.8	3.8
Q-PIV-E1-C1-Block	3.0	65.5	2.5	5.9	76.9	0.6	2.6	0.6	3.8	11.1	0.0	1.8	6.4	19.3	7.5	0.7		4.5	2.9	3.2	3.7
Q-PE-E2 (RE)-C1	4.5	77.9	0.1	2.3	84.8	0.0	1.0	0.0	1.0	8.6	0.0	1.7	3.9	14.2	0.6	0.4	1.22	6.9	6.5	3.0	8.6
Q-PE-E2 (L)-C1	1.9	70.1	0.6	3.4	76.0	0.6	1.4	0.5	2.5	10.9	0.1	2.7	7.8	21.5	4.3	0.4		4.2	3.4	2.7	4.0
Q-PE-E2 (R)-C1	8.0	64.9	3.1	1.4	77.4	0.4	0.6	0.1	1.1	8.7	0.1	4.2	8.5	21.5	2.8	0.4		4.7	2.9	1.9	4.8
Q-PE-E2 (LD)-C1	2.7	74.8	1.9	2.2	81.6	0.2	2.9	0.0	3.1	5.3	0.1	2.3	7.6	15.3	4.5	0.6	1.17	6.4	3.3	4.4	4.9
Q-PE-E2 (UD)-C1	5.5	65.4	3.1	5.0	79.0	0.0	1.0	0.5	1.5	8.2	0.1	6.3	5.0	19.5	30.3	0.6		6.4	2.4	2.4	4.5
Q-PE-E2-C1-Block	8.2	58.9	12.5	8.8	88.4	0.5	1.0	0.5	2.0	3.2	3.03	0.00	2.32	1.61	7.4	0.8		10.1	1.5	4.7	2.7

V1: Telinite, V2: Telocollinite, V3: Gelovitrinite, V4: Vitrodetrinite, L1: Sporinite, L2: Resinite + unstractural liptinite, L3: Liptodetrinite, I1: Fusinite + Semifusinite, I2: Sclerotinite, I3: Geloinertinite, I4: Detroinertinite (inertodetrinite + micrinite), MM: Mineral matter, VRr: Random vitrinite reflectance, GI: Gelification index, TPI: Tissue preservation index, GWI: Ground water index, VI: Vegetation index, *: Mineral matter free

(1–5 partings). Coal beds are usually continuous (Fig. 4g) and show iron oxide and gypsum interlamination, which indicates pyrite oxidation in outcrop (Fig. 4h) (Vassilev and Vassiliva 1996; Chou 2012), whereas fresh coal layers show considerable pyrite (Fig. 3i; Table 3).

5 Coal petrography

In order to reconstruct paleoenvironmental conditions of the mires, detailed coal petrographic characterization of the Qadir member has been carried out. Macerals, their associations, and mineral matter content can be used both for industrial purposes and for understanding the coal origin, formation, and diagenesis (Teichmüller 1986, 1989; Singh and Singh 1996; Lu et al. 2017).

5.1 Coal rank

To determine the rank of the Parvadeh coal samples, parameters such as volatile matter (daf basis) and random vitrinite reflectance values (VRr%) (Tables 2 and 4) were measured. The volatile matter ranges from 24.5% to 35.9%, with a mean of 29.7%, and vitrinite reflectance values vary from 0.79% to 1.35% with a mean of 1.13%. According to these two parameters, the coals can be classified as high volatile bituminous to medium volatile bituminous coal. Previous studies showed that the coal maturity increases from the east to the west of the Parvadeh coalfield (Shariat Nia 1994). Probably differences in subsidence and maximum burial depth caused this rank trend in the area, because there is no tectonic evidence for higher heat flow in the west.

5.2 Maceral composition

All three maceral groups, i.e., vitrinite, inertinite, and liptinite, are recorded in the Parvadeh coal seams (Fig. 5e, g, i; Table 2). Vitrinite is dominant, ranging from 59.2% to 95.4% (mean 83.6%), while inertinite varies from 3.7% to 39.3% (mean 14.5%) and liptinite from nil to 3.8% (mean 1.6%). The high vitrinite content is typical for humic coals. Vitrinite generally originates from tissues rich in cellulose and lignin, e.g. woody material, but also inner parts of leaves. Usually, in topogeneous mires permanently covered by water, vitrinite contents tend to be higher than in seasonally dry ombrogenous mires, where more inertinite and liptinite are present due to selective degradation of vitrinite (Littke 1987). Almost all the macerals and sub-macerals of the vitrinite group are recorded in the studied coal samples. Telovitrinite, in general, is the dominant sub-group, which is visible as bands and appears almost structureless (Fig. 5a, g, i).

Among the telovitrinite sub-group, the concentration of telinite is low, while collotelinite is abundant (Fig. 5 g, i, Fig. 6a). The former maceral is mainly derived from incomplete gelification of xylem and cortex tissues, and therefore its presence commonly indicates a paleoenvironment involving wood-producing plants under moist, but not permanently water-covered conditions (Diessel 1992). The cell lumens of the telinite are usually filled with mineral matter or sometimes with secondary liptinite (Fig. 5c, d). Pseudovitrinite is also present in the coals (Fig. 5b). It is characterized by higher reflectance than the normal collotelinite in the same coal and is considered a transition stage between vitrinite and semifusinite (Fig. 5e). Slits in the pseudovitrinite seem to have been created in situ due to the low-temperature oxidation of woody material and/or gasification (Mastalerz and Drobnik 2005). Also, high amounts of pseudovitrinite in the Parvadeh coals may diminish the thermoplastic properties of the coals (ICCP 1998; Taylor et al. 1998). Generally, high contents of telovitrinite imply a strong degree of cell-tissue preservation under wet, probably low-pH conditions within forested peatlands (ICCP 1998).

Some vitrinite bands show faint fluorescence properties combined with low reflectance (Fig. 5e, f). Such vitrinite is known as dark vitrinite (ICCP 1998; Singh and Singh 2013). Seemingly, this maceral formed due to the presence of micro-liptinite such as resinite in association with vitrinite (Teichmüller 1986, 1989). Vitrodetrinite and collodetrinite are the next abundant macerals of the vitrinite group (Fig. 5e, g).

Inertinite macerals with high reflectance have the same precursors as vitrinite and may suggest oxygenated, dry conditions and probably peat burning (Gentzis and Goodarzi 1990; Singh and Singh 1996; Scott and Glasspool 2007; Singh et al. 2016; Lu et al. 2017; Rajak et al. 2019). Inertinite is commonly mixed with non-oxidized constituents (Fig. 5e, g, i) and mainly comprised of fusinite and semifusinite, geloinertinite, and detroinertinite in the studied samples; however, in some samples, minor sclerotinia and micrinite are found.

Fusinite and pyrofusinite are represented by well-developed, preserved cell walls with bogen and sieve structures (Fig. 5g) and high reflectance compared to semifusinite (Fig. 5a, g). Cell lumens in these macerals are open or occupied by mineral matter. There are also macrinite and micrinite in the samples but negligible amounts. Macrinite shows amorphous irregularity, rounded to oval shape (Fig. 5h). Micrinite has been observed in these coals with white color and mixed with fine-grained mineral matter (Fig. 5c). Micrite was likely formed from liptinite macerals or small wind-borne char particles (Stach et al. 1982; Taylor et al. 1998; Scott 2002). In some samples, well-preserved secretinite has been found to occur individually as well as

Table 3 Results of Bulk-XRD analysis of coal samples

Sample name	Minerals (wt%)													
	Quartz	Calcite	Dolomite	Siderite	Kaolinite	Illite	Muscovite-illite	Chlorite	Pyrite	Anatase	Gypsum	Hematite	Albite	Orthoclase	Amorphous
Q-PI-CM-C1	6.0	0.0	0.0	1.5	5.0	14.0	0.0	0.0	3.0	0.5	0.0	0.0	0.0	0.0	70.0
Q-PI-CM-B2	13.1	0.0	0.0	0.5	6.1	22.2	0.0	0.0	3.0	0.5	0.0	0.0	0.0	0.0	54.6
Q-PII-N-C1	2.0	0.0	2.0	2.0	4.0	12.1	0.0	0.0	4.0	0.5	0.0	0.0	0.0	0.0	73.4
Q-PII-N-B1	5.0	0.0	1.0	1.0	3.0	10.1	0.0	0.0	8.0	0.5	0.0	0.0	0.0	0.0	71.4
Q-PII-N-B2	6.1	0.0	0.0	0.5	5.1	13.2	0.0	0.0	6.1	0.0	0.0	0.0	0.0	2.0	67.0
Q-PIII-E12-C1	2.0	1.0	0.0	1.0	3.0	4.0	0.0	0.0	8.1	0.0	0.0	0.0	0.0	0.0	80.8
Q-PIII-W8-B2-Block	7.1	0.0	0.0	0.5	9.1	23.2	0.0	0.0	2.0	0.5	0.0	0.0	0.0	0.0	57.6
Q-PIV-E1-C1	1.0	0.0	0.0	1.0	1.0	2.1	0.0	0.0	4.1	0.0	0.0	0.0	0.0	0.0	90.8
Q-PE-E2 (RE)-C1	1.0	0.0	2.0	1.0	0.0	2.0	0.0	0.0	4.1	0.0	0.0	0.0	0.0	0.0	89.9

in clusters (Fig. 5h). Sclerotinia is a typical maceral of the oxic environment (Scott and Glasspool 2007; Sahay 2011).

Fine inertodetrinite particles are scattered in and between vitrinite group macerals (Fig. 5e, g) with no structure and appear to have been derived from the crashing of fusinite and semifusinite.

In the coals of the Qadir member, liptinite macerals occur at low concentrations, but both primary (structured) and secondary liptinite (unstructured) macerals have been observed. Primary liptinite macerals are represented by sporinite, resinite, and liptodetrinite, and secondary liptinite maceral consist of exsudatinite and solid bitumen. The most abundant maceral among the liptinite group is resinite, which is generally oval to round shaped (Fig. 5 g, i, j). This maceral often appears as cavity or cell lumens filling within vitrinite. Resinites tend to be converted to bitumen (partly exsudatinite) during the early stages of coalification (Teichmüller 1986, 1989). The arborescent Mesozoic gymnosperms generally produce less pollen but a vast amount of resins and waxes compared to Carboniferous tropical climate flora (Diessel 1992). Sporinite occurs as an individual elongated small thread-like body usually embedded in the vitrinite matrix (Fig. 5e).

Secondary liptinite is present at an even lower concentration and related to liquid bitumen generation in the coal layers. Solid bitumen appears as amorphous and lamellar form, without any definite shape and size occurring as finely dispersed lenses together with fine-grained mineral matter impregnated by this bitumen (Fig. 5i and j and 6a and b). Exsudatinite shows strong fluorescence (Fig. 5b–e, Fig. 6b); it is usually observed at a vitrinite reflectance corresponding to the oil window (0.7–1.3) (Teichmüller 1986, Littke 1987). This maceral occurs in cleats and as cell lumina fillings (Fig. 5b–d).

Coal maceral composition in a peat-forming environment is susceptible to groundwater/sea-level oscillations, taking particularly influence on the formation of vitrinite and inertinite (Marchioni 1980; Littke 1987; Littke and ten Haven 1989; Rajak et al. 2019). Also, a common assumption in coal petrology is that inertinite-rich coals formed above groundwater level (Scott and Glasspool 2007; Zieger and Littke 2019). Thus, during times of high-water levels, maceral compositions tend to be rich in vitrinite (up to 90%); this stage refers to swamps or topogeneous mires. Under dry conditions vitrinite-inertinite assemblages are common, partly with inertinite contents above 20%–30% (Littke and ten Haven 1989; Zieger and Littke 2019). Accordingly, most of the basal coal samples in the studied section, which have high vitrinite content and less than 30% inertinite, indicate high water level coupled with reducing mire conditions within even the upper part of the peat. The high vitrinite to inertinite ratio in the studied coals (> 1, Table 2)

Table 4 Results of proximate analysis of the subsurface coal samples, daf: dry, ash free

Sample name	Moisture (wt%)	Ash (wt%)	Volatile matter (wt%)	Fixed Carbon (wt%)	Volatile matter (wt%, daf)	Fixed Carbon (wt%, daf)
Q-PI-CM-C1	0.6	29.7	22.7	47.0	32.6	67.4
Q-PI-CM-C1-Block	0.5	12.9	24.2	62.4	27.9	72.1
Q-PI-CM-B2	1.1	44.6	24.0	30.3	-	-
Q-PII-N-C1	0.6	21.4	24.8	53.2	31.8	68.2
Q-PII-N-C1-Block	1.0	38.0	25.9	35.1	-	-
Q-PII-N-B1	0.4	19.3	23.2	57.1	28.9	71.1
Q-PII-N-B1-Block	0.7	12.8	24.3	62.2	28.1	71.9
Q-PII-N-B2	0.7	29.9	24.3	45.1	35.0	65.0
Q-PII-N-B2-Block	0.5	41.4	26.1	32.0	-	-
Q-PIII-E12-C1	0.5	8.4	26.0	65.2	28.5	71.5
Q-PIII-E12-C1-Block	0.4	13.7	30.8	55.1	35.9	64.1
Q-PIII-W8-B2	0.6	21.8	27.6	50.0	35.6	64.4
Q-PIII-W8- B2-Block	1.1	50.0	30.0	18.9	-	-
Q-PIV-E1-C1	0.8	14.3	26.5	58.4	31.3	68.7
Q-PIV-E1-C1-Block	0.6	20.9	25.9	52.6	33.0	67.0
Q-PE-E2 (RE)-C1	0.5	6.6	23.4	69.5	25.2	74.8
Q-PE-E2-C1-Block	0.5	13.3	24.0	62.2	27.9	72.1
Q-PE-E2 (UD)-C1	0.5	15.1	23.0	61.4	27.2	72.8
Q-PE-E2 (LD)-C1	0.4	8.8	22.3	68.5	24.5	75.4
Q-PE-E2 (L)-C1	0.5	6.9	23.8	68.8	25.7	74.3
Q-PE-E2 (R)-C1	0.4	7.1	23.8	68.7	25.8	74.2

indicates accommodation space and peat production to be well balanced (Singh and Singh 1996; Sahay 2011; Lu et al. 2017). Relatively high inertinite contents in some coal seam horizons can result from an overall regression trend in the succession (e.g. in E coal seam) or inundation of the mire by clastic sediments and temporary rise of the water table; in this case, ash yields are high. For most coals (except tonstein ash yield), the ash yield is highly indicative for topogenous conditions during peat formation (Taylor et al. 1998). On the other hand, fusinite and semifusinite content increase towards more ombrogenous depositional conditions (Zieger and Littke 2019). Accordingly, the ratio of ash to fusinite and semifusinite (A/I) (Table 2), which was proposed by Zieger and Littke (2019), invokes the coals of Parvadeh were mostly accumulated in topogenic mires with fluctuation in water level and/or water influx, but during C1 coal seam formation, in some parts of the East Parvadeh coal mine, ombrogenous mire condition prevailed (Table 2, $A/I < 0.5$).

5.3 Mineral matter in the coals

Abundance and modes of mineral matter in coal, particularly of syngenetic/authigenic minerals, may provide useful information not only for a better understanding of the regional geological setting but also for deducing the depositional environment of peat accumulation (Diessel 1992; Ward 2002; Ketzer et al. 2003; Dai et al. 2020). According to XRD analysis, the main and common minerals in the coals are quartz, clay minerals (illite and kaolinite), pyrite, siderite, and feldspar, but minor amounts of calcite and dolomite are measured as well. In addition, negligible contents of anhydrite, barite, celestine, and chlorite are present as revealed by SEM-EDX analysis. The ash yield in the coal samples ranges from about 6.6 wt% to 50.0 wt% (Table 4).

Quartz and feldspar minerals usually have detrital sources in the coal. Quartz content varies from 1.0 wt% to 13.1 wt%, with a mean value of 4.8 (Table 3). The layered nature of these grains (siltstone to fine-grained sandstone) supports their detrital nature. The coal samples' main and most common clay minerals are illite and kaolinite (Table 3). They occur in mineral layers related to flooding (Singh et al. 2012a) of the peat (Figs. 5i and 6a and f), but also as discrete grains, in cracks and as cell lumen filling of macerals (Fig. 4b, i), the latter being related to late diagenetic crystallization. The proportion of clay minerals ranges from 2 wt% to 32 wt% in the samples (Table 3). Illite is more abundant than kaolinite and traces of chlorite were detected in some samples by SEM-EDX analysis (Fig. 6c). Illite is partly derived from syngenetic smectite being diagenetically transformed into illite in the presence of potassium. In addition, a proportion of the illite is probably diagenetic due to feldspar dissolution (Dai et al. 2018).

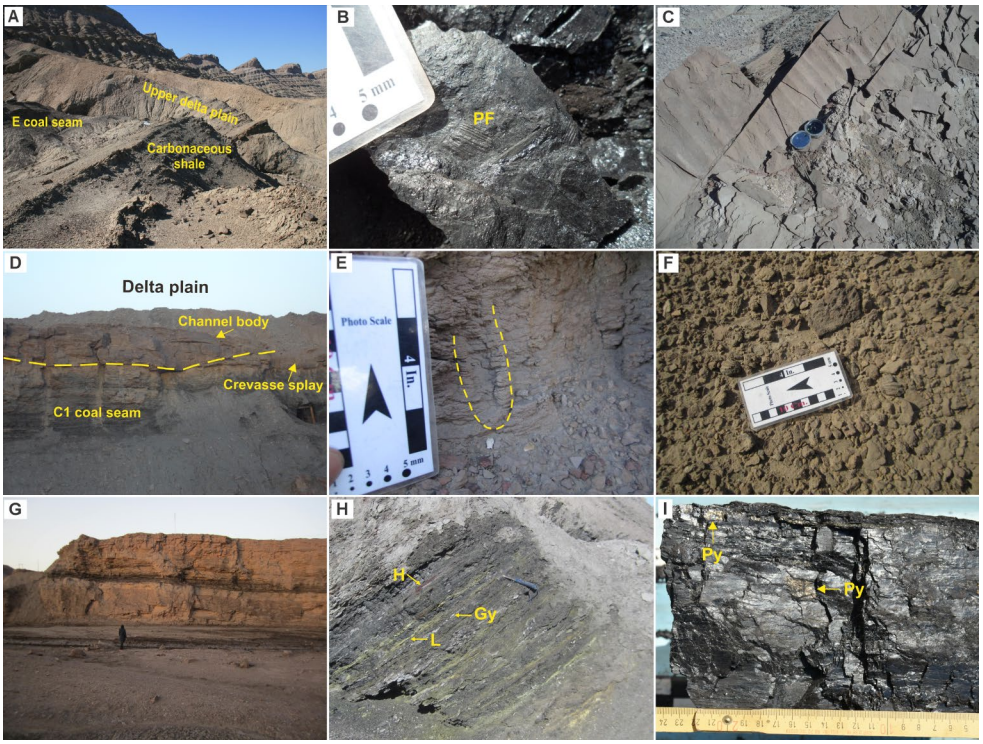

Fig. 4 Field and coal macroscopic photographs of different sedimentological facies identified along the Qadir member in Parvadeh section: **a** Fine-grained facies association of the delta plain at the upper part of the Qadir member consists of carbonaceous shale, mudstone, thin siltstone layers and coal layer (E coal seam), view toward the north **b** Close view of plant fossils (PF) on the bedding surface of coal **c** Wave-rippled surface sandstone **d** yellow dashed line marks lower erosive flat to concave upward base of sandstone channel fill sediments directly overlying coal seam in the delta plain facies association **e** Relief vertical U-tubes of *Arenicolites***f** Close view of marine shell bed bedding surface **g** Laterally continuous coal seam (C1) interbedded with a distributary channel, bay and crevasses sandstone, siltstone, and carbonaceous mudstone **h** Parallel planar layers of coal seam (B2) with oxidized pyrite as limonite (L), hematite (H) and gypsum (Gy) interlayers **i** Banded bituminous coal with well-developed cleat and pyrite (Py) mineralization

Next to illite, kaolinite is a common clay mineral in non-marine coal-bearing sedimentary rocks (Dai et al. 2018, 2020). Syngenetic kaolinite has an authigenic or/and terrigenous origin and usually occurs as pseudohexagonal plates stacked in a book-like habit (Fig. 6d). Kaolinite commonly forms under humid climatic conditions in continental sediments in slightly acidic water from aluminosilicate minerals such as feldspars and mica as well as pyroclastic glasses (Vassilev and Vassiliva 1996). Seemingly, humid conditions prevailed during the Rhaetian age in the Tabas Area resulting in both peat formation and formation of significant amounts of kaolinite.

Sulfides are represented usually by pyrite/marcasite in the Parvadeh coals, which occur as framboidal, fine disseminated, or large individual crystals (Fig. 6a, e, f). Cell and cleat filling pyrite is very common in the coals and has an epigenetic origin (Fig. 5c). The pyrite content in the samples ranges from 2.0 wt% to 8.1 wt%, with a mean value of 1.71% (Table 3). Very high pyrite contents in some samples (see Figs. 4i and 6a) indicate marine influence (Singh et al. 2010; Singh et al. 2012b), e.g. in B1 and B2 seams in Parvadeh II mine and C1 seam in Parvadeh III mine (Table 3).

Sulfur in coals mainly originates from early diagenetic microbial sulfate reduction in the peat stage (Casagrande et al. 1980; Sykes et al. 2014), while a very minor part is directly derived from plant organic matter. Sulfur mainly occurs as pyrite/marcasite (iron disulfides), while gypsum is a product of sulfide weathering at the surface. Coals overlain by marine deposits are usually strongly enriched in sulfides due to the much higher sulfate content of marine water as compared to freshwater (Stock et al. 2016). The amounts of sulfur in coals not affected by marine water are usually less than 0.5 wt%–1.0 wt% and increase to 1.0%–1.5% and more than 1.5% in coals which become subjected to minor or strong marine influence, respectively (Sykes et al. 2014; Stock et al. 2016; Zieger and Littke 2019). The average amount of organic sulfur in the coal seams in the study area is 0.8 wt% (Zadehkabir 1994a), and the mean total sulfur ranges from 1.1 wt% to 6.8 wt% (Shariat Nia et al. 1994). The average of sulfur content is usually high in the D seam, medium in B1 and C2, and low to medium in C1 and B2 (Zadehkabir 1994a; Shariat Nia et al. 1997; Zamansani et al. 2019). In particular the D seam shows a strong influence of seawater. Transgression of marine or brackish waters over a

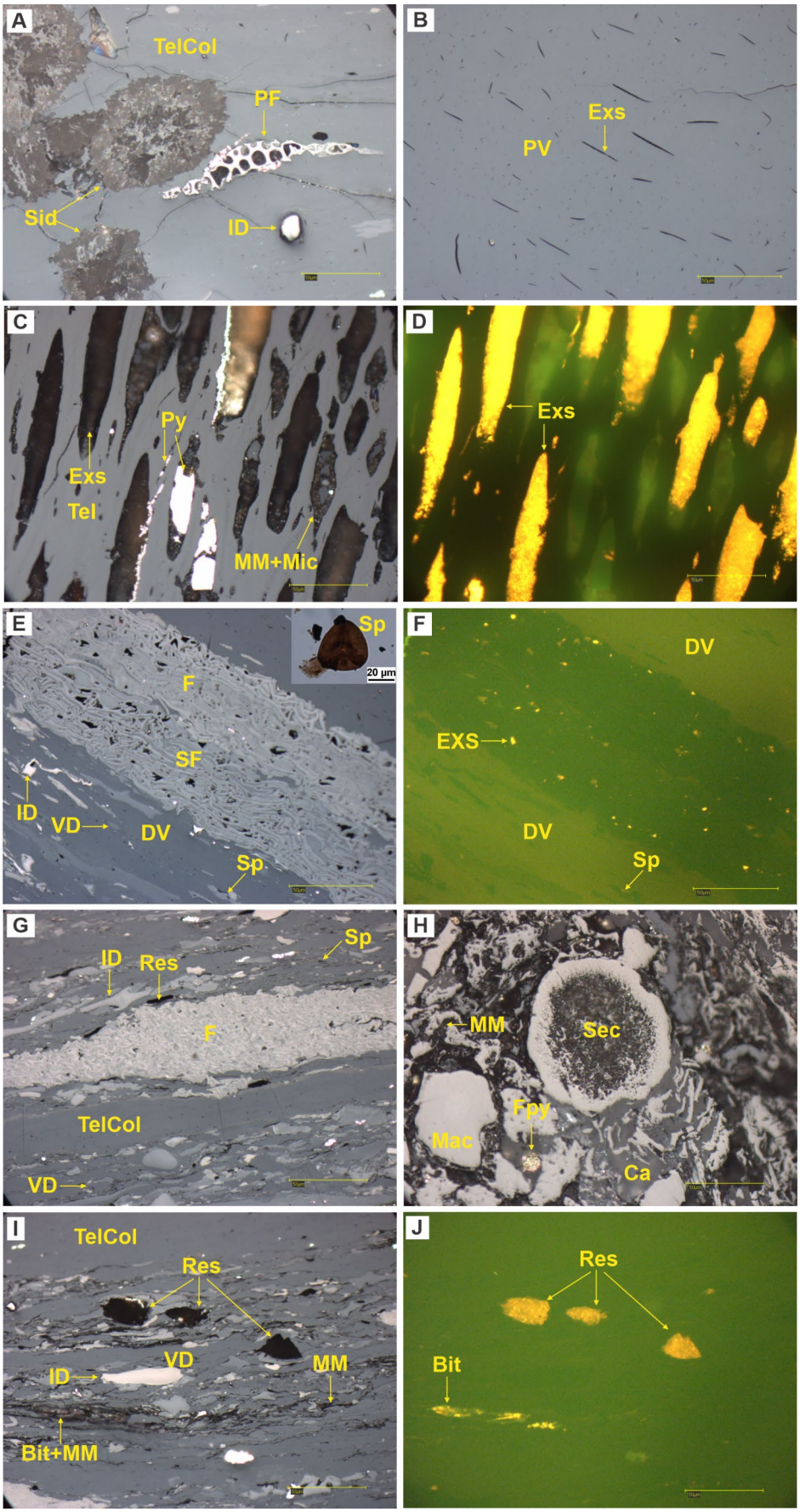

Fig. 5 Photomicrographs of macerals and minerals of the Parvadeh coal samples, the photographs taken from observations on polished surfaces in oil immersion and under white reflected light (A, B, D, E, G, H, I) and fluorescence mode following UV light irradiation (C, F, J) (scale bar is equal to 50 µm) **a** A round concretion of siderite (Sid), pyrofusinite (PF) and inertodetrinite (ID) **b** Pseudovitrinite (PV) with straight and slightly curved slit-like opening filled by exsudatinite (Exs) **c** Telinite (Tel) with lumen and fracture fillings by Exs, pyrite (Py), mineral matter (MM) and micrinite (Mic, white granules) **d** Same field as B photo, strong yellow fluorescent cell filling Exs **e** Trimacerite coal photo of transition from semifusinite (SF) to fusinite (F), Dark vitrinite (DV), ID and vitrodetrinite (VD) with angular outline and sporinite (Sp). Note spore photo under transmitted light in the upper right of the figure **f** Same field as E photo in the fluorescence mode exhibiting Exs, Sp and faint fluorescent Des **g** Fusinite with bogen structure, telocollinite (TelCol), Sp, elongated resinite bodies (Res) and mostly angular particles of ID and VD **h** Secretinite (Sec) body with foamy structure and macrinite (Mac) floating in MM and calcite (Ca) **i** Trimacerite sample with TelCol, ID, VD and very dark, isolated elliptical Res and elongate thread-like MM impregnated by bitumen (Bit) **j** Same view as I photo showing fluorescent oval Res bodies and Bit

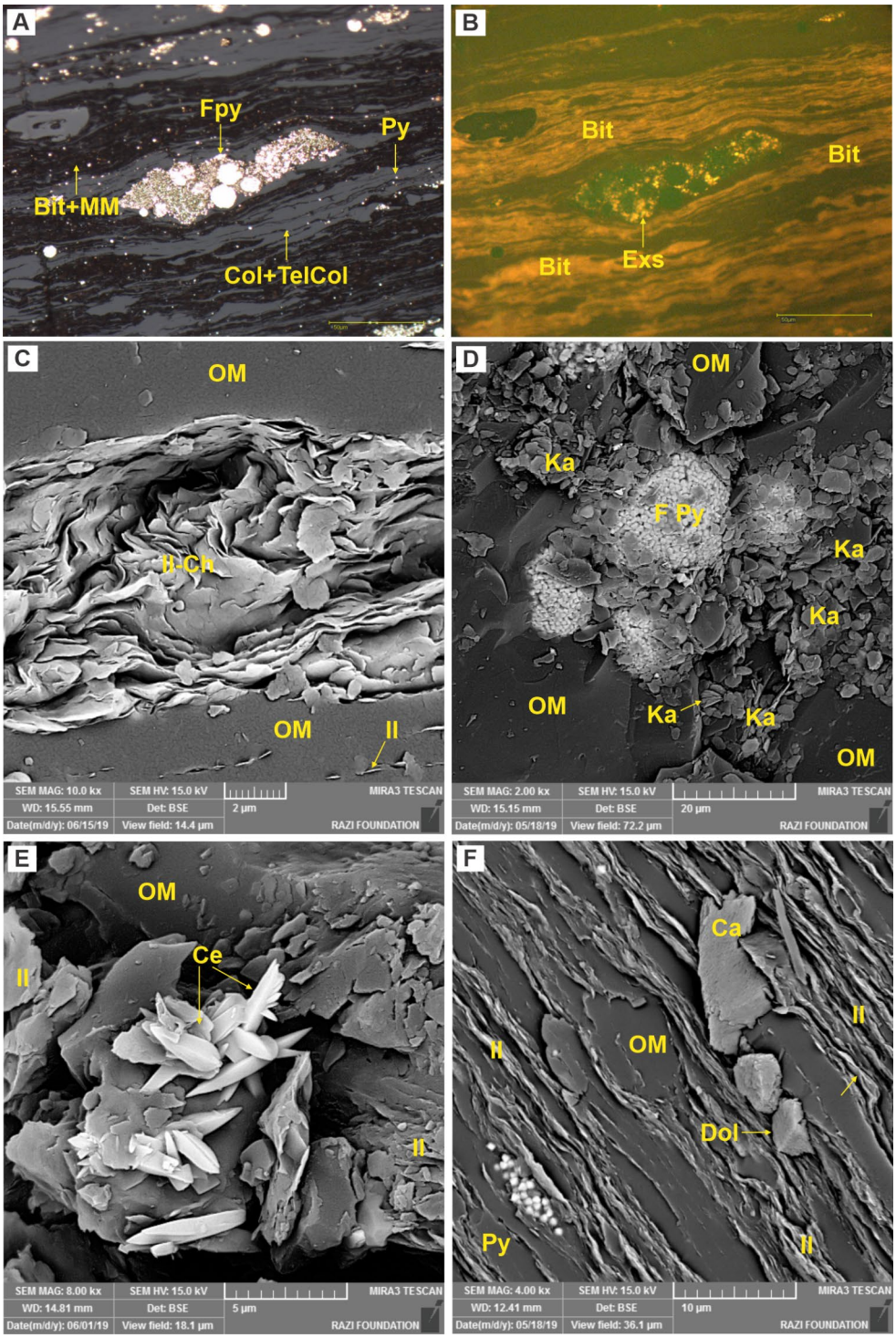

Fig. 6 Photomicrographs of macerals and minerals of the Parvadeh coal samples. Photographs were taken on polished surfaces in oil immersion and under white reflected light (A), UV light irradiation (B) (scale bar is equal to 50 µm) and back-scattered SEM (C, D, E, F). **a** Scattered and lens-like aggregates of Py crystals including syngenetic framboidal pyrite (FPy), Collinite (Col) and TelCol in a groundmass of MM and Bit with granular structure **b** Same field as A photo showing strong fluorescence of the MM which is caused by adsorption of Bit substances on the clay minerals and Exs between single Py crystals in the framboids **c** Mixed illite-chlorite (Il-Chl) clay minerals in the coal samples (OM, organic matter) with flaky and slightly crenulated shape and dust-like single plates of illite (Il) crystals oriented in OM **d** Aggregates of different size of FPy composed of small, closely packed octahederal Py crystals; booklets and platelets oriented parallel to each other with ragged edge kaolinite (Ka) crystals between them **e** Well crystalized celestite (Ce) encompassed by OM and flaky Il crystals **f** Detrital parallel Il lamina with preferable orientation along OM, single semi-idiomorph crystals of calcite and dolomite (Dol) and a small patch of lens-like euhedral Py octaheders

freshwater peat-forming environment would cause neutralization of interstitial waters at least near the top of the peat body, which increases the activity of sulfur reducing bacteria (Cecil et al. 1982). Seawater contains much more dissolved sulfate than freshwater which diffuses into the peat after flooding, where it is reduced by anaerobic sulfate-reducing bacteria (Casagrande et al. 1980; Diessel 1992; Taylor et al. 1998; Chou 2012). It seems that this kind of sulfur enrichment occurred in the D coal seam. This layer is covered by a marine fossil-rich succession (shell bed, Fig. 4f). Therefore, the high sulfur content is probably the result of the invasion of alkaline, sulfate-rich seawater into this coal seam. In contrast to the D seam, the E coal seam shows the minimum

marine influence, possibly due to this fact that the seam was formed at the end of a sea level regression period.

Seemingly, the Parvadeh peat mires were connected to the sea via the south and east, while towards the west and north, fluvio-deltaic clastic interlayers between coal seams are usually thicker and more frequent, and the coal seams show higher ash yield. Splitting is less common towards the south and east of the area, and coal layers are thinner and cleaner (Zadehkabir 1994a, b). Accordingly, the pyrite content is expected to increase in the coal seams towards the eastern and southern parts of the area.

In contrast to siderite, calcite and dolomite (Figs. 5h and 6f) formed epigenetically in the studied coal beds, i.e. they occur as cleat and cell fillings. Siderite is the common early diagenetic carbonate, and its amount ranges from 0.51% to 2.01%, with a mean value of 1.01% (Table 3). Early diagenetic siderite in the coal seams occurs as concretions (Fig. 5a); it is present to a lesser extent in cell fillings. Syngenetic siderite typically forms in environments that are consistently water-logged, organic-rich, sulfate-poor, reducing, and almost at neutral pH (7–7.8) (Castaldo et al. 1993; Dai et al. 2020).

The relations between early diagenetic siderite and pyrite can indicate the depositional environment. If early diagenetic siderite is present in coal, the coal often has a low proportion of syngenetic pyrite and vice versa (Ward 2002). However, syngenetic siderite and pyrite can also be formed under neutral to weakly alkaline conditions during peat deposition (Dai et al. 2020). However, the lateral changes in the chemistry across a peat body should also be considered, for example, synchronal siderite precipitation at the edges of the mire (higher pH) and pyrite precipitation in interior parts of the mire, where pH is low (Dai et al. 2020). Accordingly, with a high ratio of pyrite over siderite, it seems that low pH conditions prevailed in the Parvadeh peat mires. Sporadically, due to sequential invasion of fluvial water and seawater, acidic conditions were disturbed and permitted siderite mineral formation. In addition, the EDX results of Parvadeh coal siderite crystals show a considerable substitution of Mg and Ca for Fe, which indicates seawater in the coals (Dai et al. 2020).

The coal seams in the Parvadeh Area are generally characterized by medium to high ash yield (Shariat Nia 1994) (with an average of 20.8 wt%, Table 4). Seam B2 layer has the highest and seam D the lowest ash yield, and generally the coal seams have an east to west increasing parting and ash yield (Shariat Nia et al. 1997). Based on Davies et al. (2005), the proportion of detrital minerals and semifusinite is used as the main discriminator of accommodation trends within the peat mires. Therefore, it seems that accommodation space was largest in the western part of the area, where mineral and semifusinite content is high (Zadehkabir 1994a, b), probably due to higher subsidence rate (Saidi et al. 1997). Also, Tabas Block tilting toward the Yazd Block (Fig. 3) may cause an increasing coal maturity from east to west as reported by Shariat Niz (1994). The higher ash yield in the western area may indicate that the mineral matter supply into the area came from the west, which is in accordance with the prevalent west direction of current ripple marks measured in the field. The development of significant splitting of the Parvadeh coal seams may indicate a high clastic influx, disturbing peat growth in the west. The high quantity of mineral matter seems to be mainly related to flooding from fluvial distributary channels with a minor contribution by seawater. The waterborne ash and partings indicate peat development in a low-lying area near rivers as well as the inability of vegetation to baffle waterborne sediments. The ash versus total sulfur content diagram (Fig. 7) proposed by Guo et al. (2018) supports topogenic mire conditions with minor to strong marine influence and fluctuations of fresh water or brackish/sea water influx. High sulfur content is typical for coal seams influenced by marine waters or overlain by marine roofs. Petrographic studies of these seams reveal high proportions of framboidal pyrite which formed during early diagenesis as a result of microbial sulfate reduction. Such a distribution was described as typical for coals deposited in transgressive systems in proximity to the sea (Zieger and Littke 2019), which also holds true for Parvadeh Area, i.e. a paralic sedimentary environment.

6 Coal facies analysis

Organic facies analysis and coal petrographic models quantify the coal constituents and are extensively used to reconstruct the nature of ancient peat forming environments. In order to establish a correlation between coal facies indicators and the environment of peat formation, usually two parameters are calculated and plotted. Gelification index (GI) and tissue preservation index (TPI) introduced by Diessel (1986), have been used widely in coal petrography to investigate the peat mire in which a coal developed. These two indices with negligible modification (Sahay 2011) have been calculated according to the formulae:

$$\mathrm{GI} = \frac{\text{Vitrinite} + \text{Geloinertinite} + \text{Sporinite} + \text{Cutinite}}{\text{Teloinertinite} + \text{Detroinertinite}}$$

$$\mathrm{TPI} = \frac{\text{Telinite} + \frac{\text{Collotelinite}}{2} + \text{Teloinertinite} + \text{Sporinite}}{\text{Detrovitrinite} + \text{Gelovetrinite} + \text{Inertodetrinite} + \text{Geloinertinite}}$$

Due to the fact that collotelinite is regarded as semi-gelified by geochemical vitrinitization (ICCP, 1998), in the TPI formula, this maceral is divided by two. The respective diagram

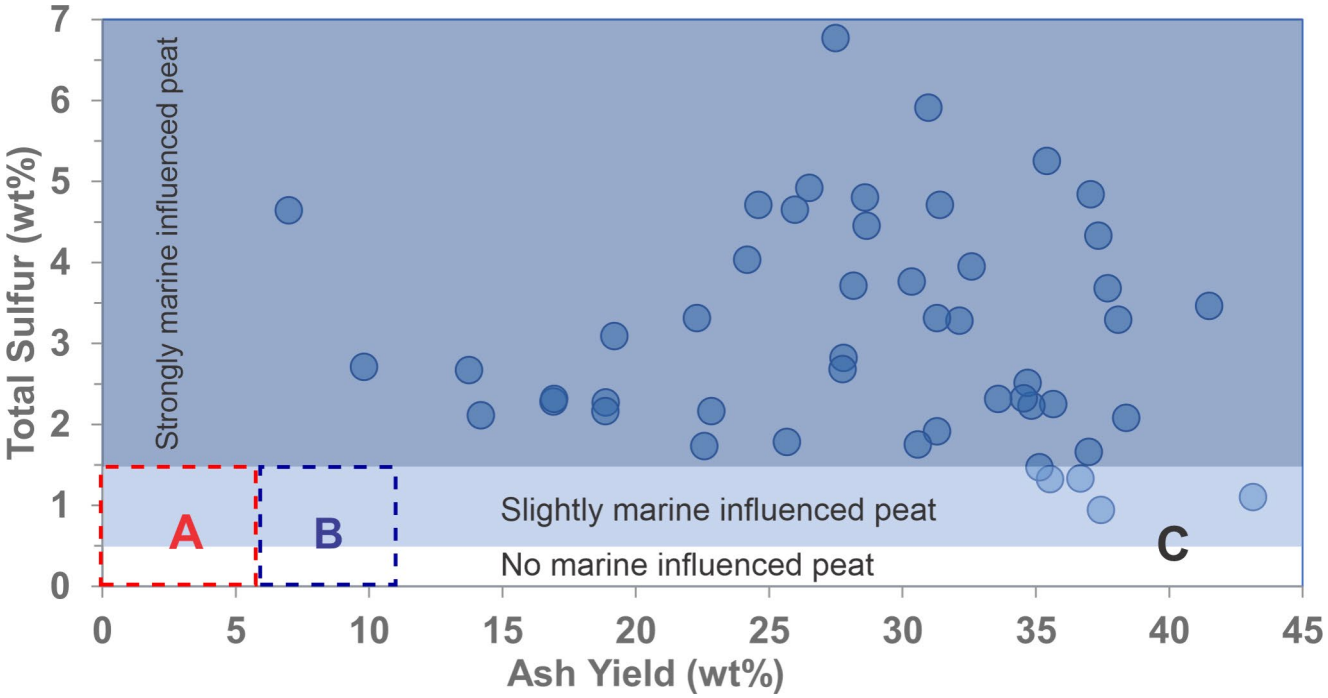

Fig. 7 Ash yield versus total sulfur diagram with interpretation of depositional peat condition (Sykes et al. 2014; Stock et al. 2016; modified after Guo et al. 2020). **A**: Ombrogenic mires, **B**: Transition area, **C**: Topogenic mires (Ash > 11%). Data from Shariat Nia et al. 1997 and Zamansani et al. 2019

of Diessel's model (1986) is divided into four quadrants on the basis of high (> 1) or low (< 1) indices (Fig. 8).

The degree of tissue preservation has commonly been reconstructed by TPI, whereas, the relative dryness (telmatic) and wetness (limnic) of the peat-forming conditions was distinguished by GI, reflecting the height of the water table during peat accumulation (Prayitno 2017). The GI ratio contrasts macerals that have undergone gelification with those that have not. The TPI ratio contrasts macerals of vitrinite and inertinite groups exhibiting original botanical cell structures with those where no botanical cell structure is visible. High TPI values reflect high percentages of woody plant particles in the original peat (Singh et al. 2011).

The Parvadeh coal samples generally show GI > 1 and TPI > 1 (Fig. 8). High TPI suggests the presence of well-preserved plant tissue and a high proportion of arboreal vegetation. Relatively high TPI is expected for coals derived from a forest swamp environment with high tree density, since intermittent dry conditions would give rise to an increased proportion of semifusinite and fusinite. High GI indicates a high and persistent water table during peat accumulation. On average, values are expected to be lower in the upper delta plain due to stronger oxidation and higher in the lower delta plain/coastal plain mires. In summary, the high GI coupled with rather high telovitrinite-based TPI in most coal seams in the Parvadeh area are indicative of a forested topogenic swamp, permanently covered by water. Considerable high ash yield in the most samples is accordance with the low-lying topogenous mires.

Another facies model of Calder et al. (1991) takes minerals/ash into account, calculating the groundwater index (GWI) and vegetation index (VI). Ash yield is considered as an important factor in coal depositional models. The GWI_{AC} and VI, which were modified slightly by Singh (2016) and Stock et al. (2016), are calculated as follows:

$$GWI_{AC} = \frac{\text{Gelovitrinite} + \frac{\text{Collotelinite}}{2} + \text{Detrovitrinite} + \frac{\text{Ash}}{2}}{\text{Teloinertinite} + \text{Geloinertinite} + \text{Telinite}}$$

$$VI = \frac{Telinite + \frac{Collotelinite}{2} + Teloinertinite + Resinite + Suberinite}{Detrovitrinite + Inertodetrinite + Liptodetrinite + Sporinite + Alginite + Cutinite}$$

Due to the fact that microscopical assessment of mineral matter content in coals is not accurate Stock et al. (2016) proposed to replace minerals counted by ash yield. Due to the density contrast between mineral matter and macerals, in the modified GWI formula (GWI_{AC}) mineral matter is replaced by half of the ash yield. Figure 8b exhibits the plotted results of the Parvadeh coal samples. In addition, since the Parvadeh coals are in medium-high maturity condition with ample of collotelinite, the GWI_{AC} is changed a little to less account the misleading homogenous vitrinite macerals.

High GWI_{AC} values clearly indicate permanently high-water tables; only rarely more oxygenated conditions transitional to raised bogs could develop. The VI indicates

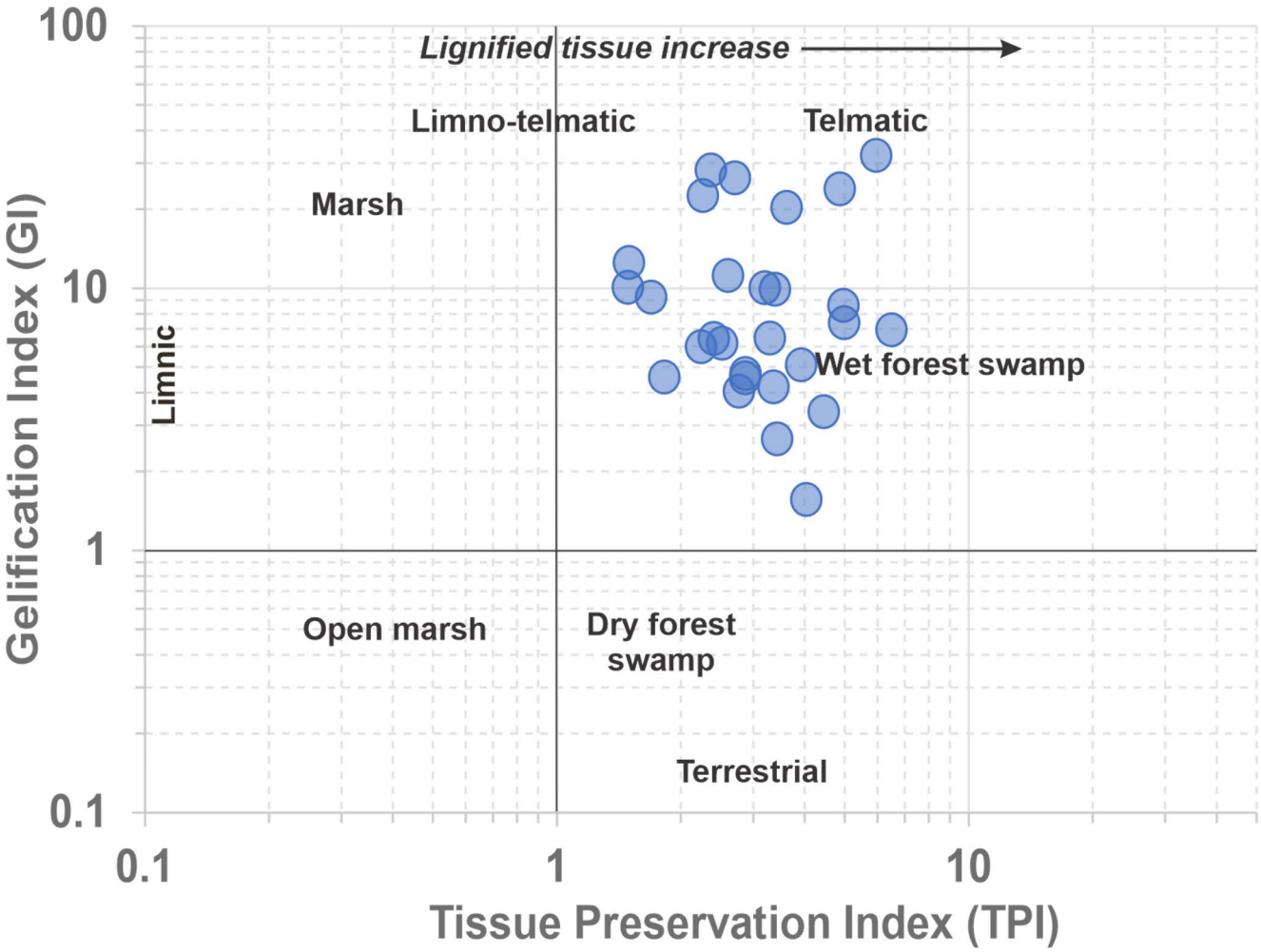

Fig. 8 Gelification index (GI) versus tissue preparation index (TPI) diagram (after Diessel 1986 and modified by Sahay 2011)

vegetation types and contrasts the macerals derived from lignin-rich plants with macerals derived from lignin-poor plants. Most of the coal samples shows high VI (VI > 3, Fig. 9a) and suggest that the coals are derived to a great extent from a vegetation with high tree density.

Coals with more than 10% mineral matter, similar to the Parvadeh coal seams, are usually associated with low-lying, rheotrophic mires and high accommodation/peat production ratios (Diessel 1992; Thomas 2002). The detrital source of most mineral matter in the studied coals may be related to inundation of the peat by distributary channel floods, i.e. overbank deposits (Fig. 9a). Rheotrophic mires d tend to be much higher in ash yield (> 10%) than raised bogs, but as a result, more mineral nutrients are available, and the vegetation is more diverse. Some parts of mires which have lower mineral matter, may be protected from clastic input by the baffling effect of thick vegetation or by topographical features (e.g. levees). Mineral matter in the form of layers usually denotes flooding episodes; under these conditions peats tend to show more frequent splits. This rheotrophic peat was formed initially on abandoned delta lobes and in interdistributary bays, as revealed by sedimentological studies in the Parvadeh Area.

As mentioned above, due to the medium-high maturity of the Parvadeh coals, it is difficult to apply the vitrinite-based facies parameters and the results can be misleading. Hence, here it is proposed using the A/I (ash/inertinite) ratio from Zieger and Littke (2019), instead of GWI_{AC}, versus VI or TPI (Fig. 9b). A/I values which plot above 0.5 are representative of topogenous mires, those below 0.5 should indicate transitional or omberogenous mires. According to this diagram (Fig. 9b), almost all of the Parvadeh coal samples plot above the 0.5 A/I line and exhibit topogenic mire condition. Only three samples of the C1 coal seam in the Eastern Parvadeh mining block are located in the ombrogenic field. In spite of possibility changing mires to each other during the geological time, eastern part of the Parvadeh have been nearest part of the deltaic environment to the marine and open water (Zadeh Kabir 1994b) and probably caused increasing oxic condition and inertinite macerals.

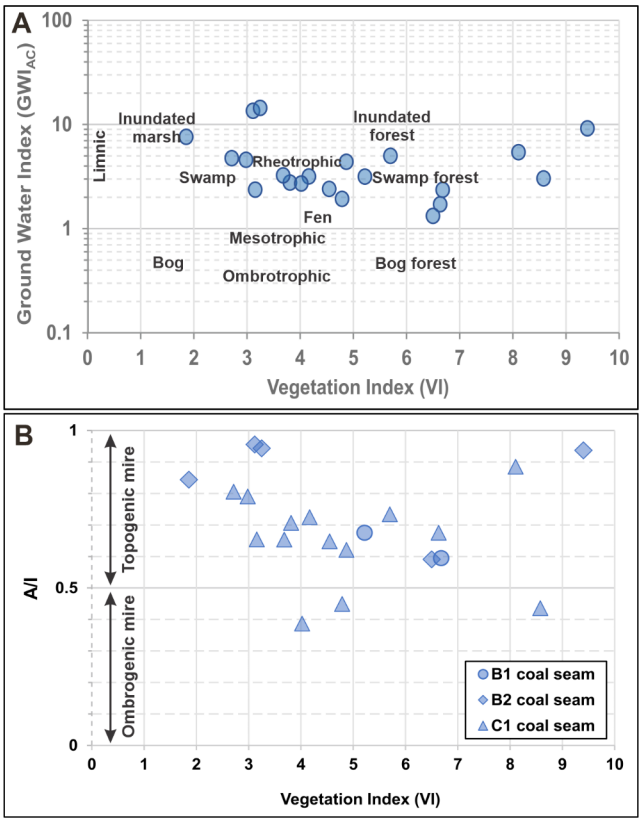

Fig. 9 Plots of coal facies indices in order to determination of depositional setting and type of mires for Parvadeh coal samples **a** Diagram of ground water influence index (GWI_{AC}) versus vegetation index (VI) (after Calder et al. 1991 and modified by Stock et al. 2016 and Singh 2016) **b** Diagram of A/I versus vegetation index (VI) (after Zieger and Littke, 2019)

Although, there are some limitations about using coal petrology indices to the determination of coal forming paleoenvironments, such as the ambiguity about the source of inertinite macerals, interpretation of tree density, gelification process, mineral matter type, and absence of liptinite macerals in the formula (Sen 2016; Scott and Glasspool 2007; Davies et al. 2005; Sahay 2011; Scott 2002), they provide useful information in combination with ash yield. Parvadeh coals are clearly from topogenous mires growing under nutrient-rich water which allowed growth of abundant trees.

7 Conclusions

Integrated sedimentological, coal petrological, and coal facies analysis of the Qadir coal-bearing member in the Parvadeh Area provide information on depositional conditions:

(1) Thick, fine-grained siliciclastic rocks containing coal seams, abundant plant fossil, dispersed organic matter, interlayers of fine-grained, cross-laminated sandstone, wavy and current ripples, and distributary channel fills imply a marine-influenced delta plain environment. During opening and spreading of the Neo-Tethys in the Rhaeto-Liassic time, a favorable climate (tropical and subtropical) provided excellent conditions for higher plant growth and -accumulation on these delta plain lobes.

(2) Probably, the coal-bearing interval at the base of the section was deposited in the lower delta plain environment. These coal seams tend to be planar with thin to medium thickness, often with splitting and high ash and sulfur content. The upper coal layer (E coal seam) was probably formed in the upper delta plain; it ranges from thin to locally thick showing lower sulfur content than the underlying coal seams.

(3) Ash yield of the coal is medium to high and minerals are mainly of detrital nature. The main ash compositions are quartz, clay minerals (illite and kaolinite), and pyrite. Syngenetic framboidal pyrite indicates a high-water table. Partly high percentages are related to inflow of brackish/marine water affecting the swamps. Water-borne ash and partings show that the coal-forming environment was in a low-lying area, probably near detrital clastic mineral sources such as fluvial and deltaic channels with high accommodation to peat production ratios. Change in acidity in conjunction with marine/brackish influxes of water also modified the pyrite/siderite ratio.

(4) The development of significant splitting and high ash yield in coal seams in the study area indicates a generally unstable depositional environment. This unstable condition during active clastic deposition is considered a function of this region's tectonic setting, i.e., close to the northern margin of the Neo-Tethys foreland basin. Also, increasing ash yield, abundance of partings, and coal rank toward the west of the area may indicate a higher subsidence rate in this direction.

(5) Coal petrography and coal facies analysis implicate forest swamp coals that originated from low-lying topogenous peatlands with rheotrophic and rarely transitional-to-ombrotrophic conditions, which extended from inter-channel lowlands towards delta lobes.

(6) The presence of distinct floor and roof boundaries, continuity of the seams, preservation of cell structure (telinite, fusinite, and semifusinite), and low amounts of detromacerals clearly indicate a autochthonous peat growth rather than allochthonous aggradation.

Acknowledgements This research is a part of the Ph.D. thesis of Tehran University in Iran. The first author would like to thank the Research Institute of Petroleum Industry (RIPI), Iran, for financial support and access to laboratory facilities. We sincerely thank Tabas Parvadeh Coal Company (TPCCO) for providing facilities during field studies and sample collection in the Parvadeh coal mines. We also would like to thank from two anonymous reviewers for comments and a careful revision.

Funding The authors have no relevant financial or non-financial interests to disclose.

Declarations

Competing interest The authors have no competing interests to declare that are relevant to the content of this article. All authors certify that they have no affiliations with or involvement in any organization or entity with any financial interest or non-financial interest in the subject matter or materials discussed in this manuscript. The authors have no financial or proprietary interests in any material discussed in this article.

Open Access This article is licensed under a Creative Commons Attribution 4.0 International License, which permits use, sharing, adaptation, distribution and reproduction in any medium or format, as long as you give appropriate credit to the original author(s) and the source, provide a link to the Creative Commons licence, and indicate if changes were made. The images or other third party material in this article are included in the article's Creative Commons licence, unless indicated otherwise in a credit line to the material. If material is not included in the article's Creative Commons licence and your intended use is not permitted by statutory regulation or exceeds the permitted use, you will need to obtain permission directly from the copyright holder. To view a copy of this licence, visit http://creativecommons.org/licenses/by/4.0/.

References

Alizadeh B, Alipour M, Hosseini SH, Jahangard AA (2011) Paleoenvironmental reconstruction using biological markers for the Upper triassic–middle jurassic sedimentary succession in Tabas Basin, Central Iran. Org Geochem 42:431–437

Brönnimann P, Zaninetti L, Bozorgna F, Dashti GR, Moshtaghian A (1971) Lithostratigraphy and foraminifera of the Upper Triassic Naiband formation. Iran Rev Micropaleontol 14:7–16

Calder JH, Gibling M, Mukhopadhyay PK (1991) Peat formation in a Westphalian B piedmont setting, Cumberland Basin, Nova Scotia: implications for the maceral-based interpretation of rheotrophic and raised paleomires. Bull Soc Geol Fr 162(2):283–298

Castaldo RA, Demko TM, Liu Y (1993) Application of sequence and genetic stratigraphic concepts to Carboniferous coal-bearing strata: an example from the Black Warrior Basin, USA. Geol Rundsch 82:212–226

Cecil CB, Stanton RW, Dulong FT, Renton JJ (1982) Geological factors that control mineral matters in coal. In: Filby RH, Carpenter BS, Ragaini RC (eds) Atomic and nuclear methods in fossil energy Research, pp 323–335

Chou CL (2012) Sulfur in coals: a review of geochemistry and origins. Int J Coal Geol 100:1–13

Cifelli F, Mattei M, Rashi H, Ghalamghash J (2013) Right-lateral transpressional tectonics along the boundary between Lut and Tabas blocks (Central Iran). Geophys J Int 193:1153–1165

Dai S, Guo W, Nechaev VP, French D, Ward CR, Spiro BF, Finkelman BF (2018) Modes of occurrence and origin of mineral matter in the Palaeogene coal (No. 19 – 2) from the Hunchun Coalfield, Jilin Province, China. Int J Coal Geol 189:94–110

Dai S, Bechtel A, Eble CF, Flores RM, French D, Graham IT, Hood MM, Hower JC, Korasidis VA, Moore TA, Püttmann W, Wei Q, Zhao L, O'Keefe JMK (2020) Recognition of peat depositional environments in coal: a review. Int J Coal Geol 219(103383):67

Davies R, Diessel C, Howell J, Flint S, Boyd R (2005) Vertical and lateral variation in the petrography of the Upper cretaceous Sunnyside coal of eastern Utah, USA-implications for the recognition of high-resolution accommodation changes in paralic coal seams. Int J Coal Geol 6:13–33

Davoudzadeh M, Schmidt K (1984) A review of the mesozoic paleogeography and paleotectonic evolution of Iran. Neues Jahrb fur Geol Palaontol - Abh 168(2/3):182–207

Diessel CFK (1986) On the correlation between coal facies and depositional environments, In: Proceedings 20th Symposium of Department Geology, University of New Castle, New South Wales 19–22

Diessel CFK (1992) Coal-bearing depositional systems. Springer-Verlag

Fielding CR (1987) Coal depositional models for deltaic and alluvial plain sequences. Geology 15:661–664

Fürsich FT, Hautmann M, Senowbari-Daryan B, Seyed-Emami K (2005) The Upper Triassic Nayband and Darkuh formations of East-Central Iran: Stratigraphy, facies patterns and biota of extensional basins on an accreted terrane. Beringeria 35:53–133

Gentzis T, Goodarzi F (1990) Petrology, depositional environment and utilization potential of late paleocene coals from the Obed-Marsh deposit, West-Central Alberta, Canada. Int J Coal Geol 16:287–308

Ghavidel-Syooki M, Yousefi M, Shekarifard A, Mohnhoff D (2015) Palynostratigraphy, palaeogeography and source rock evaluation of the Nayband formation at the Parvadeh Area, Central Iran, Iran. J of Sci Islamic Republic of Iran 26(3):241–263

Guo Q, Littke R, Zieger L (2018) Petrographical and geochemical characterization of sub-bituminous coals from mines in the Cesar-Ranchería Basin, Colombia. Int J Coal Geol 191:66–79

Hagelskamp HHB, Eriksson PG, Snyman CP (1988) The effect of depositional environment on coal distribution and quality parameters in a portion of the Highveld Coalfield, South Africa. Int J Coal Geol 10:51–77

Hashemi SM (2012) Macerals of C1 coal Seam in Parvade Coalfield (Tabas- Iran). Int J Adv Sci Eng Inf Tec 2(2):25–27

International Committee for Coal and Organic Petrology (1998) The new vitrinite classification (ICCP system 1994). Fuel 77(5):349–358

International Committee for Coal and Organic Petrology (2001) The new inertinite classification (ICCP system 1994). Fuel 80(4):459–471

ISO 7404-5 (2009) Methods for petrographic analysis of coals-part 5: method of determining microscopically the reflectance of vitrinite. Geneva, Switzerland

ISO 1171 (2010) Solid mineral fuels-determination of ash. Switzerland, Geneva

ISO 562 (2010) Hard coal and coke-determination of volatile matter. Switzerland, Geneva

ISO 589 (2008) Hard coal-determination of total moisture. Switzerland, Geneva

ISO 7404-2 (2009) Methods for the petrographic analysis of coals-part 2: method of preparing coal samples. Switzerland, Geneva

ISO 7404-3 (2009) Methods for the petrographic analysis of coals-part 3: method determining maceral group composition. Switzerland, Geneva

Kalkreuth WD, Marchioni DL, Calder JH, Lamberson MN, Naylore RD, Paule J (1991) The relationship between coal petrography and depositional environments from selected coal basins in Canada. Int J Coal Geol 19(1–4):21–76

Ketzer JM, Holz M, Morad S, Al-aasm IS (2003) Sequence stratigraphic distribution of diagenetic alterations in coal-bearing, paralic sandstones: evidence from the Rio Bonito formation (early Permian), southern Brazil. Sedimentology 50:855–877

Konon., Nadimi A, Koprianiuk M, Wysocka A, Szaniawski R, Wygladala M, Slaby E, Beygi S, Barski M (2016) Formation of intracontinental basins in the opposite corners of the Tabas block

as coeval structures controlled by transpressional faulting, Iran. Geol Soc Am Bull 128(11/12):1593–1617
Littke R (1987) Petrology and genesis of Upper Carboniferous seams from the Ruhr region, Western Germany. Int J Coal Geol 7:147–184
Littke R, Ten Haven HL (1989) Palaoecologic trends and petroleum potential of Upper carboniferous coal seams of western Germany as revealed by their petrographic and organic geochemical characteristics. Int J Coal Geol 13:529–574
Littke R, Zieger L (2019) Deposition, diagenesis and petroleum generation potential of Pennsylvanian coals and coal-bearing strata in Western Germany: a review. Z der Deutschen Gesellschaft für Geowissenschaften 170:289–309. https://doi.org/10.1127/zdgg/2019/0199
Lu J, Shao L, Yang M, Zhou K, Wheeley JR, Wang H, Hilton J (2017) Depositional model for peat swamp and coal facies evolution using sedimentology, coal macerals, geochemistry and sequence stratigraphy. J Earth Sci 28(6):1163–1177
Marchioni DL (1980) Petrography and depositional environment of the liddell seam, upper hunter valley, New South Wales. Int J Coal Geol 1(1):35–61
Mastalerz M, Drobniak A (2005) Optical properties of pseudovitrinite; implications for its origin. Int J Coal Geol 62:250–258
McCabe PJ (1987) Facies studies of coal and coal-bearing strata, In: Scott AC (ed) Coal and coal-bearing strata: recent advances. Geological Society Special Publication 32: 51–66
Miall AD (2000) Principals of sedimentary basin analysis, 3rd edn. Springer-Verlag
Mishra V, Sharma M, Chakravarty S, Banerjee A (2016) Changes in organic structure and mineral phases transformation of coal during heat treatment on laboratory scale. Int J Coal Sci Technol 3:418–428
Moinosadat SH, Razavi A (1994) Coals of Iran. Geological Survey of Iran, in Persian
Molayemat H, Mohammad Torab F (2017) Evaluation of coalbed methane potential in Parvadeh IV coal deposit in central Iran using a combination of MARS modeling and kriging. J Min Environ 8(2):305–319
Pickel W, Kus J, Flores D, Kalaitzidis S, Christanis K, Cardott B, Misz-Kennan M, Rodrigues S, Hentschel A, Hamor-Vido M (2017) Classification of liptinite-ICCP system 1994. Int J Coal Geol 169:40–61
Prayitno B (2017) Limnic condition in rheotrhopic peat type as the origin of Petai Coal, Central Sumatra Basin, Indonesia. JGEET 1(1):63–69
Rajak PK, Singh VK, Singh PK (2019) Distribution of inertinites in the early Paleogene lignites of western India: on the possibility of wildfire activities. J Geol Soc India 93(5):523–532
Repin U (1985) Stratigraphy and paleogeography of Iran's coal bearing sediments, vol 1. National Iranian Steel Company. in Persian
Sabbaghiyan H, Aria-Nasab M, Ghasemi-Nejad E (2020) The palynology of the Nayband formation (Upper Triassic) of the Tabas Block, Central Iran. Rev Palaeobot Palynol 282(104308)
Sahay VK (2011) Limitation of petrographic indices in depositional environmental interpretation of coal deposits. Cent Eur Geol 3(3):287–290
Saidi A, Brunet MF, Ricou LE (1997) Continental accretion of the Iran Block to Eurasia as seen from late paleozoic to early cretaceous subsidence curves. Geodin Acta (Paris) 10(5):189–208
Sajjadi F, Hashemi H, Borzuee E (2015) Palynostratigraphy of the Nayband formation, Tabas, Central Iran Basin: Paleogeographical and paleoecological implications. J Asian Earth Sci 111:553–567
Salehi MA, Mousavi-Harami SR, Mahboubi A, Rahimi B (2015) Lithofacies and depositional environment of the early jurassic Ab-Haji formation in outcrop and exploration boreholes of Parvadeh Coal Mine, Tabas, East Central Iran. Sci Q J Geosci 24(94):249–262 in Persian
Scott AC (2002) Coal petrology and the origin of coal macerals: a way ahead? Int J Coal Geol 50(1–4):119–134
Scott AC, Glasspool IJ (2007) Observations and experiments on the origin and formation of inertinite group macerals. Int J Coal Geol 70:53–66
Sen S (2016) Review on coal petrographic indices and models and their applicability in paleoenvironmental interpretation. Geosci J 20:719–729
Seyed-Emami K (2003) Triassic in Iran. Facies 48:91–106
Shariat Nia H (1994) Geological characteristics of the Parvadeh Region of the Tabas coal-bearing basin, Central Iran. SPG, Memoir 17: 497–509
Shariat Nia MH, Mohammadi AR, Motevali Haghi SA (1997) Exploration report of Parvadeh coal-bearing ares (general information). Natl Iran Steel Co 1:107
Singh AK (2016) Petrographic characterization and evolution of the Karharbari coals, Talcher Coalfield, Orissa, India. Int J Coal Sci Technol 3:133–147
Singh MP, Singh PK (1996) Petrographic characterization and evolution of the Permian coal deposits of the Rajmahal basin, Bihar, India. Int J Coal Geol 29:93–118
Singh PK, Singh MP, Prachiti PK, Kalpana MS, Manikyamba C, Lakshminarayana G, Singh AK, Naik AS (2012a) Petrographic characteristics and carbon isotopic composition of Permian coal: implications on depositional environment of Sattupalli coalfield. Godavari Valley, India. Int J Coal Geol 90–91:34–42
Singh PK, Singh MP, Singh AK, Naik AS (2012b) Petrographic and geochemical characterization of coals from Tiru valley, Nagaland, NE India. Energy Explor Exploit 30(2):171–192
Speight JG (2015) Handbook of coal analysis, 2nd edn. John Wiley and Sons
Stach E, Mackowsky MTh, Teichmüller M, Taylor GH, Chandra D, Teichmüller R (1982) Stach's textbook of coal petrology, 3rd edn. Gebrüder Borntraeger, Berlin
Stock AT, Littke R, Lücke A, Zieger L, Thielemann T (2016) Miocene depositional environment and climate in western Europe: the lignite deposits of the Lower Rhine Basin, Germany. Int J Coal Geol 157:2–18
Sykes R, Volk H, George SC, Ahmed M, Higgs KE, Johansen PE, Snowdon LR (2014) Marine influence helps preserve the oil potential of coaly source rocks: Eocene Mangahewa formation, Taranaki Basin, New Zealand. Org Geochem 66:140–163
Taylor GH, Teichmüller M, Davis A, Diessel CFK, Littke R, Robert (1998) Organic petrology. P. Gebüder Borntraeger
Teichmüller M (1986) Organic petrology of source rocks, history and state of the art. Org Geochem 10(1):581–599
Teichmüller M (1989) The genesis of coal from the viewpoint of coal petrology. Int J Coal Geol 12(1–4):1–87
Thomas L (2002) Coal geology, 2nd edn. Wiley-Blackwell, John Wiley and Sons,
Vaez-Javadi F (2012) Biostratigraphy of Nayband formation in Tabas, Parvadeh coal mine, according to botanical macrofossils. JSSR 46(1):113–143 in Persian
Vassilev Y (1984) Mesozoic flora fossils of Iran's coal-bearing areas, Natl Iran Steel Co, 324
Vassilev SV, Vassileva CG (1996) Occurrence, abundance and origin of minerals in coals and coal ashes. FPT 48:85–106
Ward CR (2002) Analysis and significance of mineral matter in coal seams. Int J Coal Geol 50:135–168
Wilmsen M, Fürsich FT, Seyed-Emami K, Majidifard MR (2009a) An overview of the stratigraphy and facies development of the Jurassic System on the Tabas Block, East-Central Iran. The Geological Society, London, Special Publications 312: 323–343

Wilmsen M, Fürsich FT, Seyed-Emami K, Majidifard MR, Taheri J (2009b) The Cimmerian orogeny in northern Iran: Tectono-stratigraphic evidence from the foreland. Terra Nova, Blackwell Publishing Ltd. 21(3): 211–218

Zadehkabir A (1994a) Mineral matter in coals of Iran. National Iranian Steel Company. in Persian

Zadehkabir A (1994b) Petrography of Iran's coals. National Iranian Steel Company. in Persian

Zamaniyan E, Khanehbad M, Moussavi-Haram R, Mahboubi A (2018) Lithofacies and sedimentary environment of Qadir member of the Nayband formation on Parvadeh Coal Mine region, East-Central of Iran. Geosci Q J Geosci 28(109):295–304 in Persian

Zamansani N, Rajabzadeh MA, Littke R, Zieger L, Baniasad A (2019) Organic petrology and geochemistry of triassic and jurassic coals of the Tabas Basin, Northeastern/Central Iran. Int J Coal Sci Technol 6:354–371

Zieger L, Littke R (2019) Bolsovian (Pennslyvanian) tropical peat depositional environments: the example of the Ruhr Basin, Germany. Int J Coal Geol 211. https://doi.org/10.1016/j.coal.2019.103209

Guo Q, Littke R, Sun Y, Zieger L (2020) Depositional history of low-mature coals from the Puyang Basin, Yunnan Province, China. Int J Coal Geol 221:103428

Singh PK, Singh MP, Singh AK (2010) Petro-chemical characterization and evolution of Vastan Lignite, Gujarat, India. Int J Coal Geol 82:1–16

Casagrande DJ, Gronli K, Sutton N (1980) The distribution of sulfur and organic matter in various fractions of peat: origins of sulfur in coal. GCA 44:25–32

Jalalifard M, Baniasad MR, Nazami M (2011) Biostratigraphy and age determination of Nayband Formation according to botanical macrofossils in Parvadeh Area. In 15th Conference of Geological Society of Iran: 8, in Persian

Nazemi M (2018) The role of Nayband Fault in the formation of structures and tectonic evolution of Parvadeh coal bearing area-Southern Tabas. In 4th National Iranian Coal Congress: 12, in Persian

Fallah O (2018) Tabas coal mines complex. In Iran international magazine 88

Wadsworth JA (2010) Using paralic coal as an indicator of accommodation space and correlation tool in terrestrial sediments: Examples from the Mannville Group and Falher Member. GeoCanada, Working with the Earth: 8

Publisher's Note Springer Nature remains neutral with regard to jurisdictional claims in published maps and institutional affiliations.